BIOMECHANICAL ANALYSIS OF DISTAL STENT-GRAFT–INDUCED NEW ENTRY (SINE) FORMATION IN AORTIC DISSECTION PATIENTS

TAN WEI TING

FACULTY OF ENGINEERING
UNIVERSITY OF MALAYA
KUALA LUMPUR

2019/2020

BIOMECHANICAL ANALYSIS OF DISTAL STENT-GRAFT–INDUCED NEW ENTRY (SINE) FORMATION IN AORTIC DISSECTION PATIENTS

TAN WEI TING

THESIS SUBMITTED IN FULFILMENT OF THE REQUIREMENTS FOR THE DEGREE OF MASTER IN ENGINEERING SCIENCE

**FACULTY OF ENGINEERING
UNIVERSITY OF MALAYA
KUALA LUMPUR**

2019/2020

UNIVERSITY OF MALAYA

ORIGINAL LITERARY WORK DECLARATION

Name of Candidate: Tan Wei Ting

Matric No: KGA170025

Name of Degree: Master in Engineering Science

Title of Project Paper/Research Report/Dissertation/Thesis ("this Work"): Biomechanical analysis of distal stent graft induced new entry (SINE) in aortic dissection patients.

Field of Study: Computational science

I do solemnly and sincerely declare that:

(1) I am the sole author/writer of this Work;
(2) This Work is original;
(3) Any use of any work in which copyright exists was done by way of fair dealing and for permitted purposes and any excerpt or extract from, or reference to or reproduction of any copyright work has been disclosed expressly and sufficiently and the title of the Work and its authorship have been acknowledged in this Work;
(4) I do not have any actual knowledge nor do I ought reasonably to know that the making of this work constitutes an infringement of any copyright work;
(5) I hereby assign all and every rights in the copyright to this Work to the University of Malaya ("UM"), who henceforth shall be owner of the copyright in this Work and that any reproduction or use in any form or by any means whatsoever is prohibited without the written consent of UM having been first had and obtained;
(6) I am fully aware that if in the course of making this Work I have infringed any copyright whether intentionally or otherwise, I may be subject to legal action or any other action as may be determined by UM.

Candidate's Signature Date: 25th February 2021

Subscribed and solemnly declared before,

Witness's Signature Date: 25th February 2021

Name:

Designation:

ABSTRACT

Distal stent graft-induced new entry (dSINE) is a post-treatment complication with a mortality rate of 26.1-28.6% in patients with aortic dissection (AD). dSINE creates a new path for blood flow, leading to the formation of false lumen, aneurysmal expansion, and aortic rupture. These complications necessitate re-intervention in 30-60% patients. In this study, computational approach was used to investigate potential risk factors for dSINE in aortic dissection patients. Patient-specific simulations were performed based on post thoracic endovascular aortic repair (TEVAR) computed tomography images acquired from six patients (3 dSINE and 3 non-dSINE) to analyse the correlation between anatomical characteristics and stress/strain distribution. Patient geometries were reconstructed for structural simulation. Internal pressure was applied on the inner wall of all models with restrictions of movement at all ends. Hyperelastic material models were applied. Sensitivity analysis was carried out using idealised models to independently assess the effect of stent graft length (50, 80, 100, 130, 160 and 180 mm), stent tortuosity (5˚, 10˚, 20˚ and 30˚) and wedge apposition angle (-25˚, 0˚ and 25˚) at the landing zone on key biomechanical variables. Mismatch in biomechanical properties between the stented and nonstented regions led to high stress at the distal stent graft-vessel interface in all patients, as well as shear strain in the neighboring region, which coincides with the location of tear formation. Increase in von Mises stress was observed with an increase in stent graft tortuosity (from 263 kPa at a tortuosity angle of 5^0 to 313 kPa at 30^0). Stress was further amplified by stent graft landing at the inflection point of a curve. Malapposition of the stent graft created an asymmetrical segment within the aorta, thus varying the location and magnitude of the maximum von Mises stress substantially (up to +25.9% with a +25° change in the distal wedge apposition angle). A large increase in stress occurred when the position of the maximum stress fell on the concave surface of the aorta at the distal stent graft-vessel interface. In conclusion, severe dSINE patient has

high stent tortuosity with high tortuosity angle at the distal stent-graft landing zone. The mismatch at the stent aortic wall interface induced higher stress with an increase in the tortuosity angle. Stent tortuosity and wedge apposition angle served as important risk predictors for dSINE formation.

Keywords: Distal stent graft-induced new entry (dSINE), aortic dissection (AoD), thoracic endovascular aortic repair (TEVAR), wedge apposition angle, tortuosity angle

ABSTRAK

dSINE merupakan komplikasi selepas rawatan dengan kadar kematian sebanyak 26.1 -28.6% dalam kalangan pesakit AD. dSINE mencipta aliran baru untuk pengaliran darah, menyebabkan pembentukan lumen palsu, pengembangan aneurisma and pemecahan aorta. Komplikasi sebegini memerlukan sekali intervasi dalam 30-60% pesakit. Dalam kajian ini, pendekatan komputasi telah digunakan untuk memahami faktor risiko dSINE bagi pesakit AD.Simulasi pesakit spesifik berdasarkan geometri CT 6 orang pesakit (3 SINE dan 3 tiada SINE) selepas TEVAR dianalisikan untuk memahami kaitan ciri geometri dengan pengagihan stress/regangan. Geometri aorta pesakit telah dibina semula untuk simulasi struktur. Tekanan dalaman diaplikasi terhadap dinding dalaman semua model dengan sekatan pergerakan pada setiap hujungnya. Model bahan hiperelastik telah digunakan. Analisa sensitiviti juga dijalankan menggunakan model ideal untuk mengkaji bagaimana kesan panjang stent (50, 80, 100, 130, 160, dan 180 mm), sudut bersebelahan (-25°, 0° dan 25°) dan sudut tortuositi (5°, 10°, 20° dan 30°) di zon pendaratan pada pembolehubah biomekanik. Ketidakcocokan dalam sifat biomekanik antara kawasan stent dan tanpa stent telah menyumbang kepada tekanan stress di antara muka distal stent dengan aorta untuk semua pesakit dan regangan di kawasan persebelahan merupakan lokasi formasi SINE. Peningkatan stress didapati dengan peningkatan dalam stent tortuositi (mulai dari 263kPa untuk sudut tortuositi 5^0 kepada 313kPa pada sudut 30^0). Stres ditingkatkan lagi pada pendaratan stent berada pada titik infleksi suatu lengkungan. Kesimpulannya, pesakit dSINE yang teruk mempunyai tortuositi stent yang tinggi dengan sudut tortuositi yang tinggi di zon pendaratan. Ketidakcocokan bahan antara muka aorta dengan stent menimbulkan stres yang lebih tinggi apabila sudut tortuositi meningkat. Sudut bersebelahan dan sudut tortuositi faktor risiko untuk formasi dSINE.

Kata Kunci: koyakan baru distal disebabkan stent (dSINE), pembedahan aorta (AoD), pembaikan aorta endovaskular toraks (TEVAR), sudut bersebelahan, sudut tortuositi

ACKNOWLEDGEMENTS

First and foremost, I would like to thank my supervisor Associate Professor IR Dr Lim Einly for this master project opportunity and always trying her best to provide me with sufficient resources for this project. I am also thankful to her for sustaining my stipend throughout the project and allowing me to participate in international conference in Japan. Thank you for the continuous advice to improve my presentation skills. I greatly appreciate her effort in supervising and reminding me of my progress especially at the later stage of the research journey.

Next, I would like to show my great appreciation to IR Dr Liew who is always there to supportme when I need it. She has always been a good researcher model for me to learn from, to whom students should approach for good skills, suggestion and advice. She is also the best person to seek for technical advice. Thank you for willing to advice and help me in improving my writing. I always have an efficient and helpful consultation session with her despite at minimum frequency.

My short attachment in University Malaysia Pahang is an enjoyable one, thanks for the arrangement by Dr Jamil. The consultation session is fun with both Dr Jamil and Dr Nasrul for solving technical issue of the software. Appreciation goes to Dr Jamil for answering my questions on the details for the conference and format for paper submission. Thanks to Dr Naimah, who is now a part of the UMP and was a student of Dr Einly, has contributed in providing me patient's information for further continuation of the project.

My appreciation goes to our collaborator team, Prof Xu research group in Imperial College London. I am especially thankful to Selene and Xiao Xin Kan for answering my queries regarding the methodology and for providing useful comments and feedbacks for my work. I am also thankful of Prof Shahrul from UMMC and Prof Zhong Hua Sun from the Curtin University for verification of dSINE patients.

Other than project related acknowledgement, I wish to thank everyone around me, especially my family members for tolerating my silence during my emotional low tides. There are members in the laboratory whom I wish to thanks, such as Bee Ting (graduated member), Chin Neng, Chen Onn for giving me input on random queries throughout my research journey. Emotional support that I gained from our new member, Husna at later stage of my research is helpful and enjoyable.

TABLE OF CONTENTS

Abstract iii

Abstrak v

Acknowledgements vi

Table of Contents viii

List of Figures xi

List of Tables xiii

List of Symbols and Abbreviations xiv

List of Appendices xv

CHAPTER 1: INTRODUCTION 1

1.1 Research Motivation 1

1.2 Research Objectives 2

1.3 Thesis Layout 3

CHAPTER 2: LITERATURE REVIEW 4

2.1 Classification of disease 4

2.1.1 Stanford and DeBakey classification 4

2.1.2 Kaplan-Meier curve classification 5

2.1.3 Diagnosis with medical imaging modalities and phase based aortic features

6

2.2 Treatment of AD 8

2.3 TEVAR intervention 9

2.4 Stent graft Induced New Entry (SINE) 11

2.5 Risk factors 12

2.5.1 Diameter 12

2.5.2 Taper ratio and radial force 13

2.5.3 Stent graft oversizing..15

2.5.4 Stent tortuosity 15

2.5.5 Stent graft length and spring back force...16

2.5.6 Distal stent-aorta angle at the landing zone..17

2.5.7 Chronicity/age of dissection..17

2.5.8 Wedge apposition angle 18

2.6 Summary on existing computational studies...19

2.7 Existing aortic wall material models 19

CHAPTER 3: METHODOLOGY...25

3.1 Overall workflow for CTA image post-processing 25

3.1.1 Selection of computed tomography angiography (CTA) dataset from Type B AD patients 26

3.1.2 Patients' characteristics 26

3.1.3 3D reconstruction of patient geometries 27

3.1.4 Geometrical measurements 28

3.2 Overall workflow for structural finite element analysis......................................31

3.2.1 Mesh generation 31

3.2.1.1 Mesh dependency test 32

3.2.2 Material models..33

3.2.3 Boundary conditions and simulation study 34

3.3 Sensitivity study 35

3.3.1 Generation of the idealised geometries 35

3.3.2 Model variation 36

3.3.3 Inclusion of the intercostal arteries 37

CHAPTER 4: RESULTS AND DISCUSSION 39

4.1 Geometrical measurements 39

4.2 Patient-specific simulations 40

4.3 Sensitivity analysis results 42

4.3.1 Effect of stent graft length 42

4.3.2 Effect of distal wedge apposition angle 44

4.3.3 Effect of stent tortuosity (inclusion /exclusion of intercostal arteries) 46

4.4 Discussion 49

CHAPTER 5: CONCLUSION 53

5.1 Conclusions 53

5.2 Limitations and future work 54

References 57

List of Publications and Papers Presented 65

Appendix 66

LIST OF FIGURES

Figure 2-1 Anatomical classification of aortic dissection disease by DeBakey & Stanford. Adapted from (Erbel et al., 2014) 5

Figure 2-2 Absolute movement of flap. Adapted from (Peterss et al., 2016) 8

Figure 2-3 Displacement-force relationships of the stent-grafts. Adapted from (Chen et al., 2018) 15

Figure 2-4 Peak strain values from equibiaxial tension protocol. Adapted from (Haskett, Johnson, Zhou, Utzinger, & Geest, 2010) 20

Figure 2-5 The change in microsctructure of the aortic wall on the right was due to the impact of large aggregating proteoglycan in thoracic anuerysm or dissection case compared to the normal aorta on the left. Adopted from (Cikach et al., 2018) 22

Figure 2-6 Comparison of Cauchy stress versus stretch ratio relationship of the intimal flap and normal aorta. Adapted from(Chen et al., 2018). 23

Figure 3-1 Overall workflow for the reconstruction of 3D geometries from CT images of patients. 25

Figure 3-2 3D geometry of patient 1 from CT images at post-TEVAR and 14-months follow-up with formation of SINE at the distal end 28

Figure 3-3 (a) Segmentation of patient specific geometry in Simpleware and (b) reconstructed geometry of patient specific model using the Meshmixer software. 28

Figure 3-4 Proximal diameter and distal diameter (DD) measurement of Patient 1, as calculated by the Meshmixer software. 29

Figure 3-5 Tortuosity angle measurement, as defined by 2 fitted lines for stented and unstented segments and 3 control points. 30

Figure 3-7 (a) Contour plot of aorta (b) plot of uniformly spaced centroid along the descending aorta (indicated by blue dotted line) (d) plot of centroids within the stent graft region 30

Figure 3-8 Overall workflow for structural finite element analysis. 31

Figure 3-9 (a) Idealised aortic model with different curvatures along the aorta (b) variation of wedge apposition angle; and (c) variation of tortuosity angle at the distal stent-wall interface. Blue dashed line indicates the centerline of the aorta, dark grey region represents the stent graft region while light grey region represents the unstented region. (Curve 1: A to B, Curve 2: B to C, Curve 3: C to D). 36

Figure 3-10 An example of an idealised model (tortuosity angle = 5°) with the inclusion of 10 pairs of intercostal arteries. 38

Figure 4-1 (a) Von Mises stress, (b) shear elastic strain and (c) displacement distribution for all patients. Locations with maximum values were marked with 'x', and their respective values were indicated next to 'x'. The location of new entry tear formed at follow up is indicated with red brackets for dSINE patients (patients 1-3) 42

Figure 4-2 Von Mises stress and shear elastic strain distribution for different stent graft lengths (Stent model 1: 50mm, Stent model 2: 80mm, Stent model 3: 100mm, Stent model 4: 130mm, Stent model 5: 160mm, Stent model 6: 180mm). Locations with maximum values were marked with 'x', and their respective values were indicated next to 'x'. Higher value was observed when the maximum von Mises stress occurred at the concave (CV) surface compared to the convex (CC) surface. 43

Figure 4-3 Von Mises stress distribution for stent models 2, 4 and 5 at +25˚ and -25˚ distal wedge apposition angle. CC: concave surface, CV: convex surface 45

Figure 4-4 Percentage change in the maximum von Mises stress at 25˚ and -25˚ distal wedge apposition angle when compared to 0 ˚ 46

Figure 4-5 Von Mises stress contours for models with different tortuosity angles at the distal stent-vessel interface. 47

Figure 4-6 Comparison of von Mises stress, shear elastic strain and displacement distribution with and without the inclusion of intercostal arteries, using idealised models at a 10^{o} tortuosity angle. 48

LIST OF TABLES

Table 2.1 Kaplan-Meier curves based classification standards from American College of Cardiology, IRAD and DISSECT 6

Table 2.2 Distinguishing features of acute and chronic aortic dissection based on CT imaging feature (Orabi et al., 2018). 7

Table 2.3 Clinical indicators for TEVAR interventions in aortic dissection patients....... 9

Table 2.4 Pros and Cons of intervention at the acute, subacute and chronic stage......... 10

Table 2.5 Regional linear elastic Young's Modulus values of the aorta (T. M. J. van Bakel et al., 2018).. 20

Table 2.6 Material stiffness of the 3 layers of aortic wall found in the literature. 21

Table 3.1: Demographic baseline characteristics of AD patients who underwent TEVAR (n=6). All values were expressed as mean ± standard deviation. 27

Table 3.2 Mesh dependency test results for Patient 3. 32

Table 3.3 Mesh dependency results for an idealised model... 33

Table 4.1 Post TEVAR characteristics of patients with and without dSINE. For each patient, 3 separate measurements were taken for tortuosity angle to account for the error. 40

Table 4.2 Maximum von Mises stress and shear elastic strain of the aorta with variations in the tortuosity angles (TA) at the distal stent-vessel interface/ stent tortuosity index (STI) with (WLS) and without lateral support (WOLS). 47

LIST OF SYMBOLS AND ABBREVIATIONS

AD	:	Aortic dissection
TEVAR		Thoracic endovascular aortic repair
SINE	:	Stent graft induced tear
pSINE	:	Proximal stent graft induced tear
dSINE	:	Distal stent graft induced tear
CT	:	Computed tomography
TL	:	True lumen
FL	:	False lumen
MRI	:	Magnetic resonance imaging
TOE	:	Transoesophageal echocardiography
ECG	:	Electrocardiogram
AAD	:	Acute aortic dissection
CAD	:	Chronic aortic dissection
RTAD	:	retrograde type-A dissection
STI	:	Stent tortuosity index
MR	:	Mooney Rivlin
VMS	:	Von Mises stress/ Equivalent stress
SE	:	Shear elastic strain
SS	:	Shear stress
EM	:	Elastic model
HM	:	Hyperelastic model
CTA	:	Computed tomography angiograms

LIST OF APPENDICES

Appendix A:Patient specific geometry of dSINE and non-dSINE patients at Pre-TEVAR, Post-TEVAR and follow up sessions………………… 84

CHAPTER 1: INTRODUCTION

1.1 Research Motivation

Type B aortic dissection (AD) involves a tear of the aortic wall lining that originates in the descending aorta, causing separation of the layers within the aortic wall. Minimally invasive thoracic endovascular aortic repair (TEVAR) is increasingly preferred over conventional open surgery in treating Type B aortic dissection patients. Despite being the preferred treatment option, TEVAR could lead to stent graft induced new entry tear (SINE), a post-treatment complication with a mortality rate of 26.1-28.6% (Chen et al., 2018; Q. Li et al., 2019) .

SINE creates a new path for blood flow, leading to the formation of false lumen, aneurysmal expansion, and aortic rupture (Jánosi et al., 2015). These complications necessitate re-intervention in 30-60% of patients (Pantaleo et al., 2016; Weng et al., 2013) . New intimal tears can form at the proximal tip of the stent graft (pSINE) or within 2 to 3 cm from the distal end (dSINE). The prevalence of dSINE could be as high as 81-88.1% compared to pSINE of 11.9-19% as reported in previous studies (Hughes, 2019; Jang et al., 2017; Pantaleo et al., 2016).

Due to the existence of various confounding factors in clinical studies and insufficient computational work, to date, contradictory findings have been reported with regards to the risk factors for dSINE. The existence of confounding factors in clinical studies often lead to contradictory conclusions and make it difficult to ascertain the contribution of individual parameters (e.g. aortic tortuosity, wedge apposition angle and stent graft length) on SINE formation. On the contrary, computational models, which allow reproducible experiments to be performed under identical conditions, offer the possibility to isolate the contributions of individual parameters. Carefully planned numerical studies have the potential to explain clinical observations, which would enhance our understanding of possible mechanisms leading to the occurrence of SINE.

The application of structural finite element analysis for the assessment of wall stress using patient geometries are useful to evaluate the effect of stent graft on stress distribution throughout the aortic wall (T. van Bakel et al., 2019). However, to date, limited computational studies have been performed to investigate the cause of SINE in Type B AD patients (Menichini et al., 2018, Chen et al., 2018). In particular, no studies have investigated the effect of stent graft length, wedge apposition angle and stent tortuosity on biomechanical parameters, which could lead to the formation of distal SINE in Type B AD patients. Therefore, this project aims to identify risk factors for dSINE using patient-specific finite element models of Type B AD, to help reduce the chance for dSINE formation after TEVAR.

1.2 Research Objectives

The main objective of this study is to investigate the correlation between anatomical characteristics and biomechanical variables in Type B AD patients (i.e. dSINE and non dSINE) using patient-specific finite element models, and their association with SINE formation as a result of stent wall material mismatch. Further sensitivity analysis studies are performed to evaluate the effect of stent graft length, wedge apposition angle at the landing zone and stent tortuosity on the key biomechanical variables using idealised geometries, with key geometrical parameters extracted based on patients' measurements.

The specific objectives are as follows:

i. To identify the difference between Type B AD patients with and without dSINE using geometrical analysis.

ii. To investigate the correlation between anatomical characteristics, biomechanical variables, and SINE formation using finite element structural analysis.

iii. To analyse the effect of stent graft length, wedge apposition angle at the landing zone and stent tortuosity on the key biomechanical variables using sensitivity analysis on idealised geometries, with key geometrical parameters based on patients' measurements.

1.3 Thesis Layout

This thesis starts with an introduction to the scope of the project, which includes Research Motivation, Research Objectives and Thesis Layout.

Chapter 2 provides a background literature section of the topic, which includes disease classification, diagnosis methods, treatment approaches and distal stent graft induced new entry (dSINE). In addition, a review on previously published clinical as well as computational studies on the risk factors for SINE was presented.

Chapter 3 provides a detailed explanation on the methodology used to post-process medical images from Type B AD patients, as well as workflow for finite element simulations.

All results are reported in Chapter 4. The first section of Chapter 4 focuses on comparing geometrical characteristics and computational results for dSINE and non-dSINE patients. The next section of Chapter 4 focuses on additional simulation results, which include the effect of the inclusion of intercostal arteries, as well as the effect of material models. All results are discussed at the last section of this chapter.

Summary of findings, conclusions, study limitations, and recommendations for future work are presented in Chapter 5.

CHAPTER 2: LITERATURE REVIEW

2.1 Classification of disease

Aortic dissection (AD) occurs when there is a tear at the aortic wall lining, thus splitting the wall into layers as the blood flows through. The dissected aorta has a complex geometrical appearance due to the variation in size, number and location of tear. The false lumen (FL) and true lumen (TL) diameters vary based on the volume of blood flowing through. The naming of this disease is generally based on the anatomical location of the tears. However, for better intervention planning for the treatment of the disease, the temporal course classification is introduced. The classification systems used are Stanford, DeBakey, and Kaplan, as discussed in the following sections.

2.1.1 Stanford and DeBakey classification

The two anatomical classifications are Stanford and DeBakey classification, as shown in Figure 2.1. When the dissection occurs at the ascending aorta and arch, it is referred to as Stanford Type A AD; any dissection beyond that region is named as Stanford Type B AD. For the DeBakey classification, cases involving both aorta regions are Type Ⅰ whereas for those affecting the ascending aorta or descending aorta only, they are Type Ⅱ and Type Ⅲ, respectively. In other words, Type B AD is referred as Type Ⅲ AD. DeBakey Type IIIa involves the descending thoracic aorta whereas DeBakey Type IIIb involves the thoracoabdominal aorta.

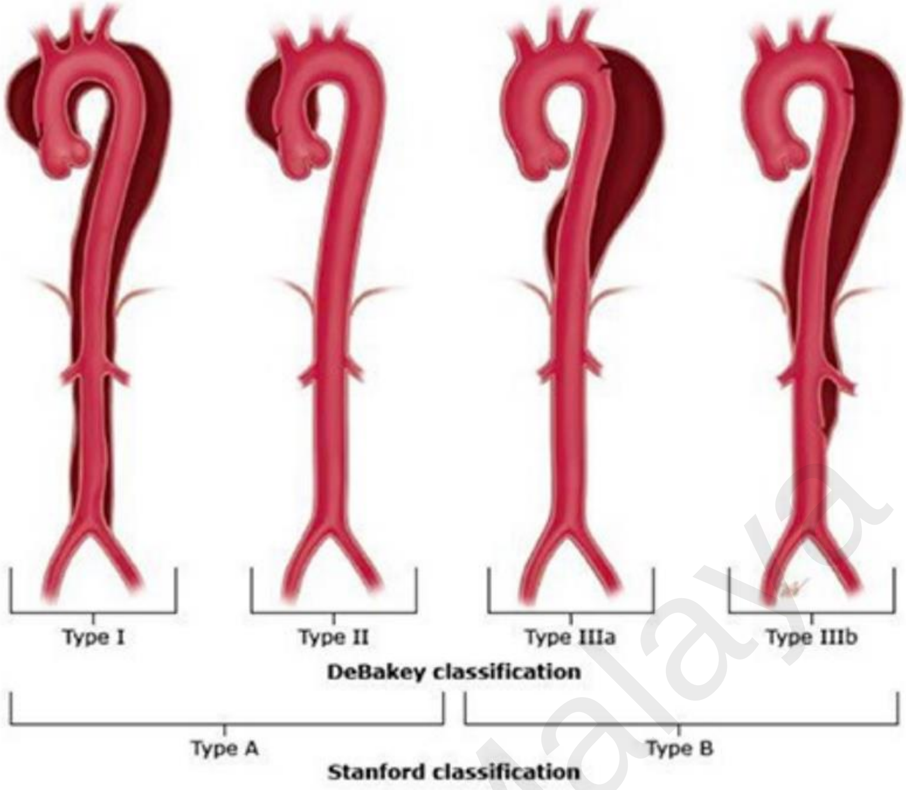

Figure 2-1 Anatomical classification of aortic dissection disease by DeBakey & Stanford. Adapted from (Erbel et al., 2014)

2.1.2 Kaplan-Meier curve classification

Temporal classification is based on inflection points of the Kaplan-Meier curves. This classification is used to ease medical doctors and clinicians in identifying the stages of the disease for intervention. It is described by four distinct time periods derived from the inflection points. Various classification standards based on Kaplan-Meier curves have been put to use to-date as shown in Table 2.1. The terminology of acute dissection and chronic dissection in this thesis follows the American College of Cardiology classification standards.

Table 2.1 Kaplan-Meier curves based classification standards from American College of Cardiology, IRAD and DISSECT

Classification standards	Hyperacute	Acute	Subacute	Chronic
1. American College of Cardiology/American Heart of the society of Thoracic Surgeons Endovascular Surgery Task Force	-	≤ 14 days from the onset of symptoms	-	≥14 days from symptom onset
2. IRAD Classification System (Booher et al., 2013)	< 24 hours	2 to 7 days	8-30 days	> 30 days
3. DISSECT/ VIRTUE Registry Investigators (Dake, Thompson, van Sambeek, Vermassen, & Morales, 2013; Investigators, 2014)	< 24 hours	Within 2 weeks	2 weeks up to 3 months	> 3 months/ 90 days

2.1.3 Diagnosis with medical imaging modalities and phase based aortic features

From the clinical perspective, there are signs for the disease at different temporal phases (e.g. acute, subacute,and chronic). Patients with acute dissection have mediastinal haematoma and severe abdominal pain whereas for chronic dissection patients, they are expected to have widened mediastinum, sudden onset of interval chest pain and aneurysmal dilation.

AD is usually diagnosed using medical imaging with the contrast-enhanced computed tomography (CT) angiography as the most commonly used modality (Nienaber & Powell, 2011). Chest radiography and CT are first used followed by magnetic resonance imaging (MRI) or transoesophageal echocardiography (TOE) (Barry J. Doyle & Norman, 2016).

The latest clinical imaging study by Orabi suggests that there is a distinctive morphological difference between acute dissection and chronic dissection patients. They use geometrical features (refer Table 2.2) in CT scan images to determine the disease phase of the patient (Orabi et al., 2018). The mobility and appearance of the intimal flap is of latest research interest.

Table 2.2 Distinguishing features of acute and chronic aortic dissection based on CT imaging feature (Orabi et al., 2018).

Acute aortic dissection (AAD)	Chronic aortic dissection (CAD)
• periaortic confluent soft tissue • opacity curved dissection flap • highly mobile dissection flap	• thick dissection flap • false lumen outer wall calcification • FL thrombus • dilated FL • tear edges curling into the FL

The intimal flap is the torn away part of the aortic wall lining and forms a membrane between the true and false lumen. The changes of the mobility of the intimal flap as the disease progresses has been reported by Peterss et al., 2016 (refer Figure 2.2). The intimal flap mobility appears to be highest at the hyper acute stage. Mobility of the flap can be identified within the first week of the acute stage and slowly loses its mobility afterward (Peterss et al., 2016). The intimal flap dynamics likely appear low after three months (chronic stage).

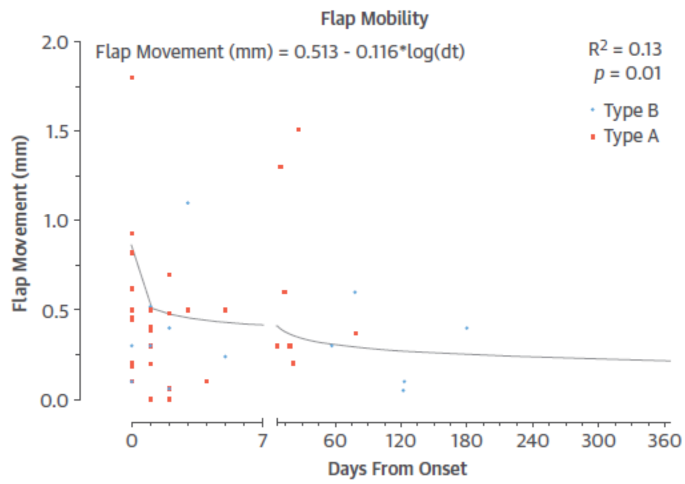

Figure 2-2 Absolute movement of flap. Adapted from (Peterss et al., 2016)

2.2 Treatment of AD

The three main treatment options for AD patients are medical treatment with drugs, open surgery and thoracic endovascular aortic repair (TEVAR). Medical treatment uses drugs to lower the blood pressure. Open surgery or endovascular repair (inserting stent graft) covers or occludes the primary entry tear to shut off the false lumen. Most commercially designed stent grafts are of standard sizes which is often insufficient, therefore patient-specific custom designed stent grafts appears to gain increasing usage among clinicians. The technique may also be modified according to individual clinical cases. For example, existing applied techniques are modified TEVAR (Zhu et al., 2018), mixed treatment, hybrid arch elephant trunk repair or change in procedure sequence that are performed for better treatment outcomes.

For severe cases where the tear is located at the ascending aorta (near the heart) for Stanford Type A AD patients, open surgery is usually performed (Nienaber & Powell, 2011). As for non-complicated Type B AD patients, medical treatment is the preferred treatment option. TEVAR, which is minimally invasive, has been found to produce aortic remodeling and reduce aorta related mortality compared to medical therapy in uncomplicated Stanford Type B. For complicated Stanford Type B, especially elderly

AD patients (Aoyama, Kunisawa, Fushimi, Sawa, & Imanaka, 2018), the suitability of the type of treatment is still in debate.

2.3 TEVAR intervention

Few clinical indicators for TEVAR interventions based on observation of the patient's symptoms at different disease phases are listed in Table 2.3. However, there is debate on the optimal timing of interventions, as listed in Table 2.4. Some literature suggest subacute as the ideal time point (Trimarchi & Eagle, 2016). This is further supported by Li et al., 2016,'s findings which reported lower cumulative re-intervention rate and major complication rate in subacute groups compared to the acute and chronic phase. Moreover, the cumulative mortality of subacute dissection patients is lower than acute and chronic patients. Generally, earlier intervention is preferred due to higher capability of aortic remodeling (Fanelli et al., 2016) and lesser physical interference due to lower flap mobility.

Table 2.3 Clinical indicators for TEVAR interventions in aortic dissection patients

Acute dissection patients	Chronic dissection patients
• aortic rupture (hemothorax, hemomediastium) • malperfusion syndrome (acute limb ischemia, bowel ischemia, renal ischemia) • persistent pain for > 3 days and hypertension refractory to medical treatment	• presence of complications as impeding rupture and organ ischemia or unstable blood pressure • maximum short-axis thoracic aortic diameter > 55mm and rapid growth (10mm/year) of thoracic aorta

Table 2.4 Pros and Cons of intervention at the acute, subacute and chronic stage

Stage of intervention	Pro	Cons
Acute	Active remodeling	Dissecting membrane is fragile
Subacute	Similar remodeling ability as acute Dissecting membrane is less fragile as the dissecting flap matures and stabilizes, thus allowing safer delivery of stent	Increase in overall aortic diameter due to the relatively less change in the false lumen compared to acute stage. (Zhou et al., 2018)
Chronic	Low mobility of flap	Low rate of remodeling (D.-l. Li et al., 2016) Full thrombosis is less likely to occur

The endovascular outcomes are assessed based on technical success in correct deployment of stent grafts, complete exclusion of the primary entry tear and induction of favourable morphological modelling (Patterson et al., 2014). Favourable characteristics of morphological remodeling are progressive thrombosis of the false lumen, contemporary enlargement of the true lumen, absence of enlargement of the total aortic diameter and 5 mm reduction in maximal descending thoracic aorta diameter at follow-up.

Although TEVAR is commonly preferred over open surgery due to its non-invasive nature for aortic treatment, there are other risks involved, especially when treating AD patients. The complex geometry of AD patients has twisted lumens with high curvature region and the lumen diameter varies highly among the segments. Limited tapering of the existing stent graft might lead to adverse treatment outcomes as the graft may not conform to the patient's geometry due to large tapering difference. The long term performance of stent grafts in patients is a concern for AD patients (Canaud et al., 2019).

Device-related post-TEVAR complications such as type I endoleak, SINE, and retrograde type-A dissection (RTAD) (Sze et al., 2009) can occur. The incidence of these complications is believed to be due to procedural or operational factors or the progression of the disease itself. Furthermore, AD patients with genetically altered aortic wall properties (Marfan syndrome) were suggested to have an increase in the risk of tearing complications after the insertion of the stent. Fragile dissection membrane or diseased tissue has disordered microstructure and thus making it more prone to tearing. However, with the introduction of recent distal first intervention, the incidence of SINE is expected to be lower even for patients with tissue disease.

2.4 Stent graft Induced New Entry (SINE)

SINE is a new tear caused by the stent graft, and is not created by natural disease progression or any iatrogenic injury from the endovascular manipulation (Dong et al., 2010). Stent graft induced new entry can occur at both proximal and distal regions of the stent. Proximal SINE usually occurs at the proximal tip of the stent whereas distal SINE can occur at 2 - 3 cm distal to the stent graft end.

A new intimal tear formed after primary TEVAR provides a new path for the blood to flow and thus reforming the false lumen. As a result, SINE can lead to pseudoanuerysm, re-dissection or rupture. Treatment for proximal SINE is open repair whereas for dSINE, distal TEVAR extension or open repair are normally performed (Hughes, 2019). Re-intervention is required to improve survival of patients with SINE complications but patient death due to dSINE complication after the re-intervention can occur as well (Q. Li et al., 2019).

There is more reported post-TEVAR complications such as dSINE (Hughes, 2019) in AD patients. Similar stent graft technical specifications might lead to different stent graft and aortic wall interaction outcomes due to high variation in the aortic geometry of individual aortic dissection patient. Most of the procedural improvements appear to have limitations and short term effectiveness (Q. Li et al., 2019) in the prevention of the occurrence or development of complications as the risk factors for distal SINE are not fully understood or verified.

2.5 Risk factors

The potential risk factors for distal SINE found in the literature are the aortic diameter, taper ratio, stent oversizing ratio, stent graft radial forces, stent graft length, distal stent-aorta angle and age of the dissection or chronicity, of which some literature provides contradictory findings. More recent computational simulation and clinical review studies have suggested stent tortuosity index (Menichini et al., 2018) and wedge apposition angle (Lescan et al., 2019) as the latest risk factors for SINE. The subsequent sections will discuss the terms related to the risk factors for distal SINE.

2.5.1 Diameter

The importance of diameter can vary with stages (diagnose, treatment, recovery tracing). Expansion of the aortic diameter was used as an indicator for the risk of rupture and thus an indicator for intervention or re-intervention. For AD patients, the aortic diameter is also used as an indicator for the appropriate selection of the size of the stent graft (Kawatani et al., 2015). The wrong sizing due to incorrect diameter measurement at the sealing zone might lead to migration or endoleak (Grande & Stavropoulos, 2006).

Proximal and distal stent end diameter measurements are important as the interaction of stiffer stent graft region with the uncovered aortic wall could lead to tear. After the intervention, the measurement of the expansion or shrinkage of the aortic diameter represents the degree of aortic remodeling in patients (C. Y. Huang et al., 2013).

In some clinical studies, aortic diameter is a risk factor for SINE but for many others, the correlation is not significant. Based on computational simulation theories, a larger aortic diameter gives higher wall stress (Ziganshin & Elefteriades, 2019) although diameter is not the only determining factor for stress (other factors include curvature, contact dynamics). However, the pulsatile nature of the blood flow causes dynamic changes of the aorta and thus single time point measurement has limitations in suggesting the size for stent graft for the intervention when using conventional CT single time point scanned image (T. van Bakel et al., 2019)

2.5.2 Taper ratio and radial force

Taper ratio of the true lumen is the ratio of the difference of the landing zone diameter, (i.e. the difference of proximal and distal landing diameter) to the proximal landing diameter (Canaud et al., 2019). The initial design of the stent graft for TEVAR treatment has limited tapering, considering high tapering nature of the aorta in AD patient. High taper ratio has been found the risk factor for SINE as clinicians believe the radial stress exerted by the stent graft onto the aortic wall upon expansion could lead to high stress and thus tearing of the highly tapered aorta.

However, there are contradictory findings which show both significant (C.-Y. Huang et al., 2016; Jang et al., 2017; Jánosi et al., 2015) and no significant difference (Weng et al., 2013) in the taper ratio of SINE and non-SINE groups. (Lescan et al., 2019) found higher taper ratio in non-SINE patients compared to SINE patients, which is contradicting others' findings (C.-Y. Huang et al., 2016; Jang et al., 2017; Jánosi et al., 2015; Weng et al., 2013) .

According to Qing Li et al., 2019, the intimal flap cannot withstand the radial force compression exerted by the stent graft in long term and will have a higher tendency to develop dSINE. In some discussions, it is stated that considering the radial force of the stent (not commonly available in technical specification sheets) might improve treatment results. The displacement to radial force relation for different brands of stent grafts has been reported by Chen et.al., 2018 (refer Figure 2.3) in recent years.

Flap could come in different thickness and stiffness. The re-apposition pressure of the flap by the stent, therefore could vary and should be considered during TEVAR. For chronic patients, higher re-apposition pressure is required to reduce the false lumen diameter. Selection of stent graft based on radial force is to be further investigated to improve effectiveness of treatment.

Although one study shows lower reccurrence of distal SINE in patients who undergo re-intervention with stent of higher taper ratio, no clinical significance difference was found compared to commonly used stents of lower taper ratio (Q. Li et al., 2019). Furthermore, the study by Lescan et al., 2019 utilized delay non-bare stent graft with four zones of varying radial force for TEVAR treatment, some of the patients however still develop SINE.

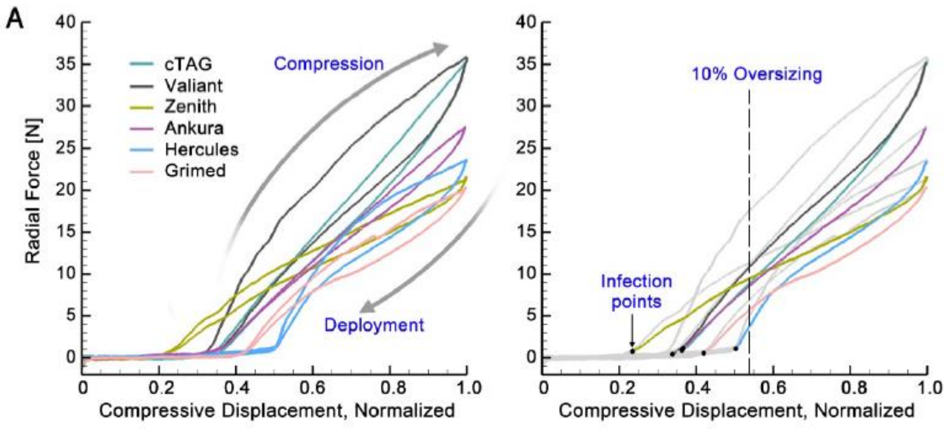

Figure 2-3 Displacement-force relationships of the stent-grafts. Adapted from (Chen et al., 2018)

2.5.3 Stent graft oversizing

Careful stent-graft selection (appropriate sizing) and implantation planning are described to reduce complication risks (Chen et al., 2018). Clinically, stent graft oversizing is related to endoleak and massive adverse effects throughout the disease phase (Fanelli et al., 2016). Oversizing ≥ 20% significantly suggests the need for re-intervention (Faure et al., 2014) and greater oversizing might lead to endograft collapse (infolding) and incomplete sealing. Oversizing of less than 20% is clinically recommended to be rectified by using the non-dissected midaortic arch as the reference diameter when choosing the stent graft during reintervention. A computational study by Ma, Dong, Wang, et al., 2018 confirmed higher aortic wall stress when an oversized stent was inserted. Although many past clinical studies (Jánosi et al., 2015; Pantaleo et al., 2016; Weng et al., 2013) pointed out excessive distal oversizing as a risk determinant of SINE (Canaud et al., 2019), a recent study (Lescan et al., 2019) however found no significant difference in the oversizing value for both SINE and non-SINE groups.

2.5.4 Stent tortuosity

Aortic tortuosity, which is the curvature of the endograft (Spinella et al., 2018), also plays an important role in the formation of dSINE. This was suggested by a computational study comparing stent tortuosity of two patients by (Menichini et al., 2018) but the small number of sample cannot lead to a concrete conclusion.

Meanwhile, in a study based on 22 patients who underwent preoperative, 1-month and 1-year post-TEVAR follow-up computed tomography angiography (CTA) scans, the mean aorta curvature at the distal stent graft landing zone was found to increase (Spinella et al., 2018). The observed variations in these parameters with time in individual patients could be caused by age-associated shrinking of body size and lengthening of aorta (Belvroy et al., 2019).

2.5.5 Stent graft length and spring back force

Stent graft length is identified as a significant risk factor based on recent clinical reviews (Q. Li et al., 2019). Most of the clinical findings relate the usage of the short stent (with a length of 145 mm and 165 mm) to a high incidence of dSINE (Lescan et al., 2019; Q. Li et al., 2019; Q. Li et al., 2015; Ma, Dong, Fu, et al., 2018). Although longer stent length is suggested to reduce the incidence of dSINE (Q. Li et al., 2019), a clinical study by (Jánosi et al., 2015) however opposed this finding, concluding that there is no significant difference in stent length between dSINE and non-dSINE groups.

Spring back force describes the tendency of the passively bent stent to recoil and straighten after the implantation. A shorter stent graft has a higher spring back force due to the leverage effect of the lesser curve of the arc on the device. dSINE risk is higher when a short stent is implanted in the aortic arc at high curvature region. This implantation exerts unwanted forces or changes in the stent tortuosity or aorta geometry. When the landing is at the thoracic aorta / proximal region of the aortic arc, the stent graft tends to have higher drag force acting upwards, and this elastic recoil of the rigid stent graft might lead to aneurysmal degeneration. The use of connecting bars to restrict mobility of the spring was said to reduce the flexibility of the aorta and avoid potential kinking and twisting due to less prominent spring back force. In a patient specific simulation by Ma

(Ma et al., 2018), higher stress is observed at the proximal region of the stent due to the presence of a connecting bar instead of the increase in stent length (Ma, Dong, Wang, et al., 2018). Although the results suggested the stress at the proximal region is less affected by the length of the stent graft, there has been little investigation on the distal landing stress.

2.5.6 Distal stent-aorta angle at the landing zone

Positioning the stent graft into a straight aortic region is expected to have less risk of dSINE development. In Janosi's study, distal stent-aorta angle was found to be significantly different between the patients with and without dSINE (149.08 ± 15.09° vs. 166.72 ± 12.47°, P < 0.005). After TEVAR, the angle between the distal end of the stent and the stretch of the aorta (distal stent-aorta) was associated with tendency of the rigid stent to spring back and straighten, and therefore the risk of dSINE.

2.5.7 Chronicity/age of dissection

Qing Li et al., 2019 pointed out chronicity as a significant dSINE risk factor. In contrary, the review by Canaud et al.,2019 showed no difference in three studies, except for a single study where dSINE was found to occur more frequently in patients with chronic dissection. This contradicting result was further demonstrated by one recent study which found no significant difference in the occurrence of dSINE between acute and chronic groups (Lescan et al., 2019).

The interaction of the semi-rigid stent graft with the pulsatile aortic wall could induce stress at the interface due to the mismatch of material properties (T. van Bakel et al., 2019). At the acute stage, the intimal flap allows the expansion of the stent due to its higher mobility and less stiffness compared to the chronic stage (Q. Li et al., 2019). Thus, the incidence of SINE is expected to be less at the acute stage (Q. Li et al., 2019). Lower mobility in the intimal flap together with a fragile and stiff aortic wall in chronic AD patients are more likely to succumb to tearing (Ziganshin & Elefteriades, 2019). Clinical discussions (Canaud et al., 2019) implied higher incidence of SINE in chronic patients but the actual risk factors, (e.g. wall stiffness, flap mobility) has not been numerically verified.

There were studies analysing the risk factors based on the disease stage. For example, SINE was more profound in chronic patients compared to acute patients (Fanelli et al., 2016). The chronic aorta is more fibrotic and therefore is stiffer, less expandable and has less capacity for remodeling of the true lumen than acute patients. In chronic dissection, expansile force of the oversized stent graft (which is a risk factor) can lead to friction injury on the rigid wall and more frequent occurrence of new intimal tears and therefore SINE. Besides that, chronic AD subjects have a higher number of stent grafts and are also most likely to be treated with significantly longer stents compared to acute cases. Meanwhile, there are geometrical characteristic changes from acute to chronic with overall increase of internal diameter and the degree of curvature of the aorta.

2.5.8 Wedge apposition angle

Wedge apposition angle is defined as the angle between the plane perpendicular to the graft and the aortic centerline in the distal landing zone (Lescan et al., 2019). The wedge apposition angle is found to be lower in acute dissection patients (< 14 days since diagnosis) compared to chronic dissection patients (> 14 days since diagnosis) and there is an increase in its mean value only in chronic groups during follow-up. This is the only clinical study that recently pointed out a short stent with a high wedge apposition angle is a risk factor for SINE; however, no computational simulation has been performed to verify this risk factor. The presence of the wedge apposition is dependent on the arch geometry and the stent graft's length. Shorter grafts frequently end in the curved region and may lead to higher pressure exerting onto the dissection flap.

2.6 Summary on existing computational studies

Several computational studies (Chen et al., 2018; Ma, Dong, Wang, et al., 2018; Menichini et al., 2018) have investigated factors leading to SINE in AD patients using patient-specific geometries. Persistently high aortic wall stress has been identified as the main risk indicator for SINE. A recent study by Ma, Dong Wang, et al., 2018 found that oversizing could contribute to the formation of SINE through high stress concentration at the stent-vessel interface, which is suggested to be caused by angled contact between the end of the proximal bare stent graft and the aortic wall. Another study (Chen et al., 2018), on the other hand, proposed a method to identify the risk of dSINE based on stent-induced vessel deformation. While most studies have focused on identifying correlations between biomechanical parameters and the risk of dSINE formation, the only computational study that looked into the contribution of geometrical parameters is that by Menichini et al., 2018. In their study, two patient geometries (one with dSINE and another without) with distinct anatomical characteristics in terms of aorta-driven stent graft tortuosity, curvature and thoracic aortic length, were analysed (Menichini et al., 2018; T. M. van Bakel, Figueroa, van Herwaarden, & Trimarchi, 2018) using a simplified linear elastic model. To date, there is a lack of computational studies which focus on the effects of stent graft length, wedge apposition angle and aortic tortuosity at the distal landing zone and their role in the formation of distal SINE. Different degree of stent wall material mismatches also has not been investigated as encountered at different disease stages (acute versus chronic) where the stiffness of the aorta could be different.

2.7 Existing aortic wall material models

Generally, at the macroscale level, the aorta stiffness varies throughout the aorta. Different axial and circumferential stiffness are found at different regions of the aorta. The descending thoracic aorta appears to be stiffer in the axial direction compared to the ascending thoracic aorta (Roccabianca, Figueroa, Tellides, & Humphrey, 2014). Recent studies by van Bakel et al., 2018 reported region-based material stiffness of the aorta with aneurysm (refer Table 2.5).

Table 2.5 Regional linear elastic Young's Modulus values of the aorta (T. M. J. van Bakel et al., 2018)

Aorta region	Linear elastic stiffness /MPa
Aortic root	1.68
Ascending aorta	1.68
Right coronary artery	3.20
Left coronary artery	3.20
Brachiocephalic trunk	2.00
Left common carotid artery	2.00
Left subclavian artery	2.00
Distal aorta	1.84
Ascending aortic aneurysm	2.00
Descending aortic aneurysm	2.56
Endograft	55.2

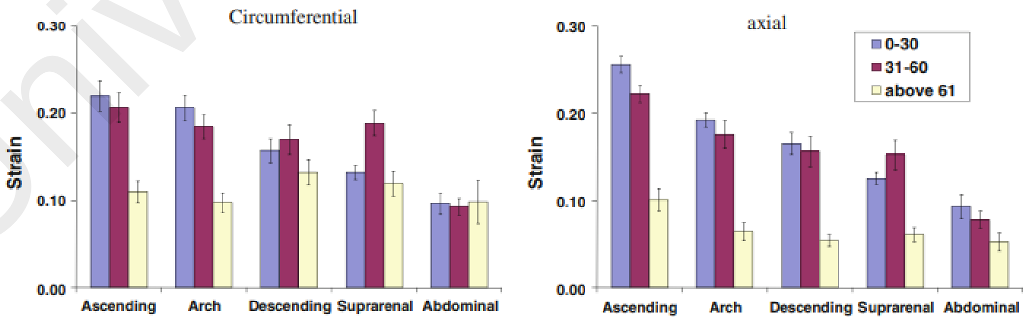

Figure 2-4 Peak strain values from equibiaxial tension protocol. Adapted from (Haskett, Johnson, Zhou, Utzinger, & Geest, 2010)

Moreover, the aorta gets stiffer due to aging. In Haskett's study, a higher degree of anisotropy is found for circumferential compliance compared to axial compliance, especially in the aging group (Figure 2.4). Older groups have lower compliance in both directions compared to the younger groups. There is also a gradual decrease in compliance along the aorta from the ascending aorta the abdominal region (Haskett et al., 2010).

At microscale level, the aorta wall is separated into three main layers: innermost layer (intima), medial layer (media) and outermost layer (the adventitia) (Ziganshin & Elefteriades, 2019) and therefore different material models exist in the literature whereby different stiffness was assigned to the intima, media and adventitia as shown in Table 2.6.

Table 2.6 Material stiffness of the 3 layers of aortic wall found in the literature.

Layers	(Simsek & Kwon, 2015)	(Gao, Watanabe, & Matsuzawa, 2006)
Intima	0.522 MPa	2.98 MPa
Media	1.565 MPa	8.95MPa
Adventitia	1.043 MPa	2.98 MPa
Degenerated zone	0.078 MPa	-

When viewed microscopically, the aortic wall is made up of anisotropic elastin and collagen fiber (Yu, Wang, & Zhang, 2018). This leads to fiber material models (Lu, Chen, Qi, & Wang, 2018; Yeh, Rabkin, & Grecov, 2018), such as 2-fiber models (Ahuja et al., 2018; García-Herrera et al., 2012) and 4-fiber models for microscopic level computational studies.

When affected by disease, the microstructure of the aortic wall is disturbed and this is reflected in the changes of the macroscopic material characteristic of the wall (Cikach et al., 2018). This changes is due to the accumulated glycosaminoglycans (GAGs) that sequester water and induce swelling within the intra-lamellar spaces of the medial layer of an artery, leading to stress concentration that can trigger damage and delamination at the microscopic level (Ahmadzadeh, Rausch, & Humphrey, 2018).

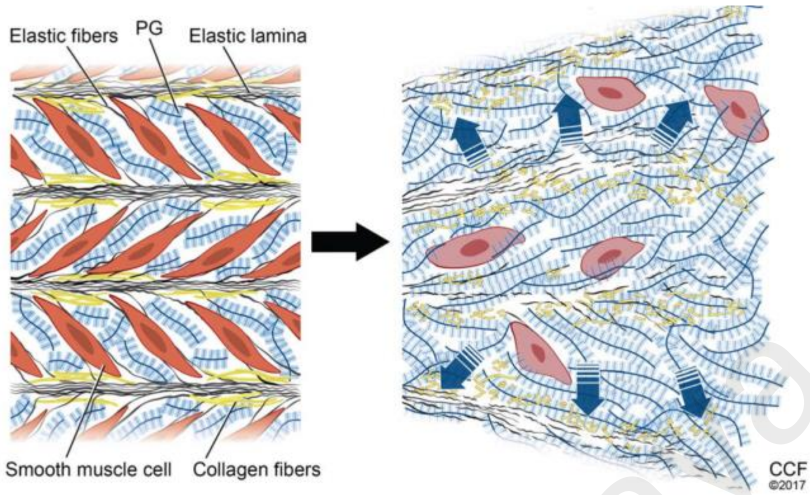

Figure 2-5 The change in microsctructure of the aortic wall on the right was due to the impact of large aggregating proteoglycan in thoracic anuerysm or dissection case compared to the normal aorta on the left. Adopted from (Cikach et al., 2018)

Most of the existing material models were based on aneurysm tissue properties instead of the actual human intimal flap tissue properties. To date, only one study has actually derived its material models from aortic dissection patients (Chen et al., 2018), specifically they are the first group to establish the material stiffness of the intimal flap from aortic dissection Type A patients. The isotropic hyperelastic model (modified Mooney-Rivlin strain energy density function) was used and they found that the flap appears to be stiffer relative to the normal aorta (refer Figure 2.7). Most of the other studies either adopt healthy descending thoracic tissue (García-Herrera et al., 2012) or animal tissue.

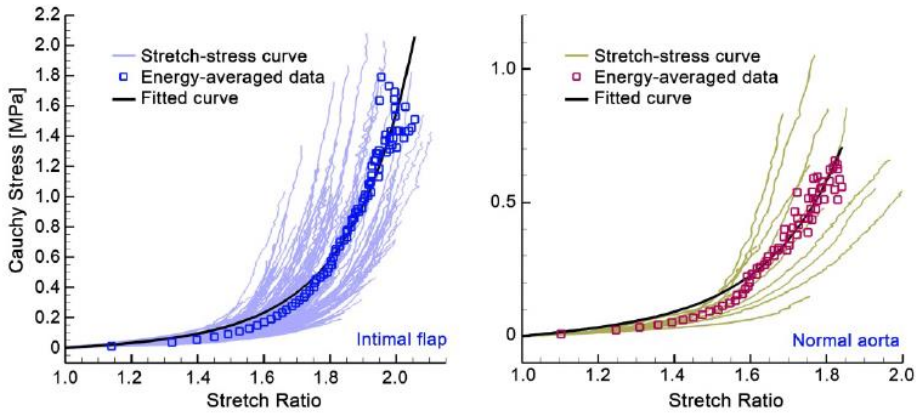

Figure 2-6 Comparison of Cauchy stress versus stretch ratio relationship of the intimal flap and normal aorta. Adapted from(Chen et al., 2018).

Some of the previous material model implementations are based on animal tissue such as porcine (Ahuja et al., 2018) and bovine due to difficulty in retrieving sufficient human diseased tissue for experimental tensile tests. However, there are studies showing that for certain conditions or age groups, the stiffness of the animal aortic model is not a good representative of the stiffness in human aortic model (de Beaufort et al., 2018). Therefore, careful selection of the material model and assumptions are suggested. For example, in the Beaufort study, the stiffness of young porcine aortic tissue shows good correspondence with human tissue aged <60 years and therefore chosen to represent the aortic stiffness of this age group rather than human aortic tissue aged >60 years which have been found much to be stiffer.

Other material models found in existing computational studies are linear elastic and isotropic hyperelastic. Specifically, tor a healthy aorta , the linear elastic Young Modulus's value ranges from 0.84 MPa (Gao, Guo, Sakamoto, & Matsuzawa, 2006) to 1.2 MPa (Brown et al., 2012; Z. Li & Kleinstreuer, 2005) as well as hyperelastic models in some studies (Shang, Nathan, Sprinkle, Fairman, et al., 2013; Shang, Nathan, Sprinkle, Vigmostad, et al., 2013). The reported stiffness is 2 MPa for a healthy aortic valve (Ranga, Mongrain, Biadilah, & Cartier, 2007). For aneurysm (abdominal) or dilated aorta (Ziganshin & Elefteriades, 2019), the material stiffness in between 3 (Nathan et al., 2011) and 4.66 MPa (Giannakoulas et al., 2005; Z. Li & Kleinstreuer, 2005, 2007; Thubrikar, Al-Soudi, & Robicsek, 2001) is reported. For diseased tissue such as Marfan syndrome, 3 MPa (Singh, Xu, Pepper, Treasure, & Mohiaddin, 2015) is applied. A relatively higher stiffness of 5 MPa is applied for retrograde type A AD in one of the latest studies (T. M. van Bakel et al., 2018).

With respect to the inconsistency of finding on clinical risk factor for dSINE, this project compares both risk factors (taper ratio, stent tortuosity, stent graft length) and biomechanical parameters (stress, strain) of dSINE and non-dSINE using patient-specific finite element models of Type B AD. With finite element models, this study investigates the effect of the characteristic of distal landing zone (curvature or straight, with apposition angle and without) of the stent graft on the biomechanical stress induced by the mismatch at the interface. Further sensitivity study investigated the effect of stent tortuosity/tortuosity angle on the stress induced at the distal stent wall interface due to material mismatch. which could lead to the formation of dSINE in Type B AD patients.

CHAPTER 3: METHODOLOGY

In the first section of this chapter, workflow for CTA image post-processing was presented, which includes patient selection, patient characteristics, steps for 3D geometry reconstruction and geometrical measurements. This was followed by workflow for structural finite element analysis, which comprises mesh generation, selection of material models and settings of boundary condition. Finally, methodology adopted for sensitivity analysis was presented.

3.1 Overall workflow for CTA image post-processing

The overall workflow for the selection of patients' geometries, reconstruction of 3D geometries from CT images of patients as well as post-processing to obtain geometrical measurements is shown in Figure 3.1. First, CT dataset from six patients, containing three patients with dSINE and three patients without dSINE, were chosen. The CT images were then segmented to obtain the true and false lumen contours. 3D geometry reconstruction was then performed from the short-axis stack of CT images, and geometrical measurements, such as diameter, stent graft length and taper ratio were then obtained through post-processing.

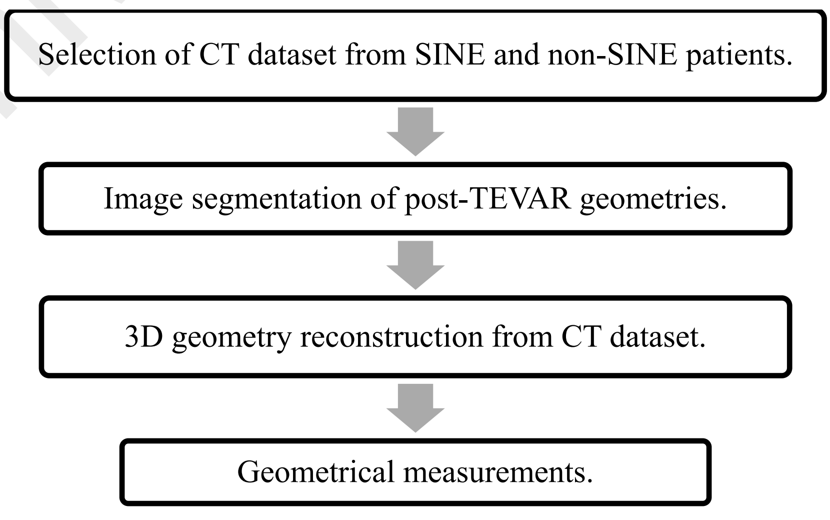

Figure 3-1 Overall workflow for the reconstruction of 3D geometries from CT images of patients.

3.1.1 Selection of computed tomography angiography (CTA) dataset from Type B AD patients

The study population consists of Stanford Type B AD patients who underwent CTA scanning before and after TEVAR treatment. The CTA images were obtained from Sir Charles Gairdner Hospital, Perth, Western Australia between 2004 and 2015, with ethical approval (Approval number: SCI-31-14, HREC No: 2014-115). Three patients who developed dSINE (determined from their follow up CTA images), along with three other who did not develop dSINE, were selected. The images were anonymized before further analysis. All Type B AD patients diagnosed with dSINE (N=3), who had at least three scanning time points, i.e. pre-TEVAR, post-TEVAR and follow-up scan between 6 – 18 months were included in this study as the dSINE group. An equal number of non-dSINE patients (N= 72 3) with comparable range of age, proximal and distal landing diameter as well as stent length were selected as the control group. All the patients were implanted with the Valiant thoracic stent grafts (Medtronic, Minneapolis, MN, USA).

3.1.2 Patients' characteristics

Patient 1 (P1) developed dSINE within 2 months after TEVAR, with continuous increase in aortic diameter from 7.5 to 15 months. dSINE is formed 3 months after TEVAR in Patient 2 (P2) but remained stable with no sign of aortic expansion at 17 months and 44 months follow-ups. Patient 3 (P3) developed dSINE within 14 months post-TEVAR and had severe aneurysmal dilation. Two of the dSINE patients, P1 and P2 have short stent length (≤165 mm) of 150 mm and 140 mm, respectively, whereas P3 has a long stent of 200 mm. Two of the non-dSINE patients (P4 and P5) have long stent length (≥ 165) of 180 mm and 200 mm, respectively, whereas P6 has a short stent graft length of 135 mm. The demographic baseline characteristics of all patients included in this study are listed in Table 3.1.

Table 3.1: Demographic baseline characteristics of AD patients who underwent TEVAR (n=6). All values were expressed as mean ± standard deviation.

Characteristics	dSINE (n=3)	Non-dSINE (n=3)
Age	61.0 ± 9.2	57.7 ± 16.9
Acute: Chronic ratio	2:1	3:0
Male: Female ratio	2:1	2:1
Stent graft length, mm	163.3 ± 32.1	170.0 ± 33.3
Average maximum follow- up months	24.3 ± 17.0	6.3 ± 4.2

3.1.3 3D reconstruction of patient geometries

Three-dimensional patient-specific geometrical models of the post-TEVAR aorta were reconstructed from CT images of the AD patients (Figure 3.2). Image segmentation and reconstruction were performed using SimpleWare ScanIP (Version 3.2, SimpleWare Ltd., Exeter, UK) and MeshMixer (Version 3.5.474, Autodesk, San Rafael, CA, USA), respectively (refer Figure 3.3). Structural wall models of the aorta were built by extruding the reconstructed lumen surface with a uniform wall thickness of 1.4 mm for the aortic wall and 2.3 mm for the composite stent-wall (Menichini et al., 2018). Please refer to Appendix A for more examples of the patients' STL geometries (pre TEVAR, post TEVAR and follow up).

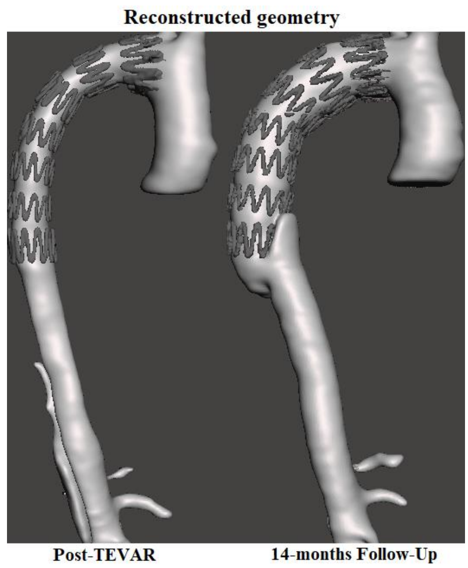

Figure 3-2 3D geometry of patient 1 from CT images at post-TEVAR and 14-months follow-up with formation of SINE at the distal end

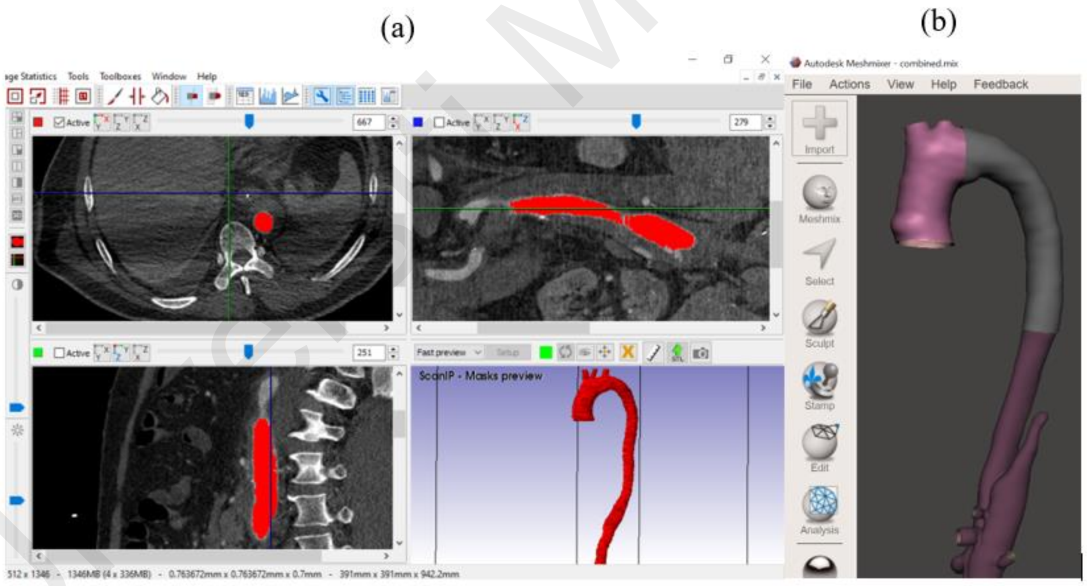

Figure 3-3 (a) Segmentation of patient specific geometry in Simpleware and (b) reconstructed geometry of patient specific model using the Meshmixer software.

3.1.4 Geometrical measurements

Several geometrical parameters were computed from the reconstructed geometries, including aortic diameter at the proximal and distal end of the stent-vessel interface (refer

Figure 3.4), taper ratio, stent tortuosity index (STI), and tortuosity angle at the distal stent-vessel interface. Taper ratio was defined as follow:

$$\text{Taper ratio} = \frac{\text{Proximal landing diameter} - \text{Distal landing diameter}}{\text{Proximal landing diameter}} \tag{3.1}$$

STI was defined as follow:

$$STI = \frac{\text{Stent graft length}}{\text{Distance between proximal and distal end of the stent graft}} \tag{3.2}$$

Tortuosity angle at the distal stent graft-vessel interface was measured as the angle (green) between the stented and unstented segments (angle subtended by 2 fitted line and 3 control points, as shown in Figure 3.5 and Figure 3.9) (Belvroy et al., 2019).

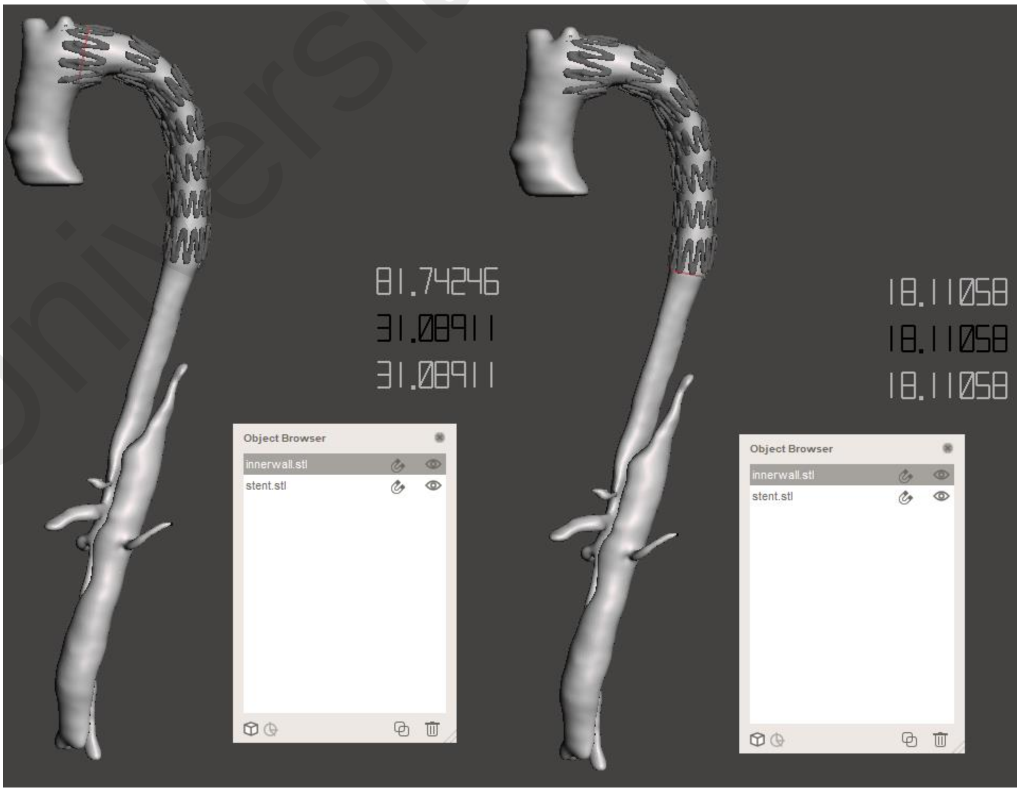

Figure 3-4 Proximal diameter and distal diameter (DD) measurement of Patient 1, as calculated by the Meshmixer software.

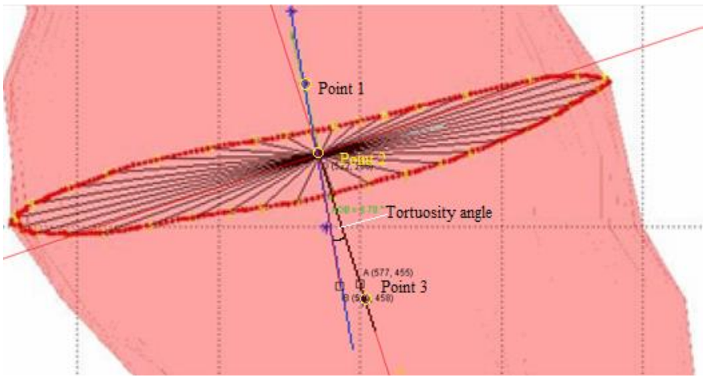

Figure 3-5 Tortuosity angle measurement, as defined by 2 fitted lines for stented and unstented segments and 3 control points.

To measure the stent-graft length, the aorta was first contoured from the CT scans. The centroids of the aorta were subsequently computed from the surface points of the aorta (Figure 3-7a) and interpolated into uniformly spaced centroids using spline interpolation (Figure 3-7b). The stent-graft length was then extracted as the summation of Euclidean distances between all the adjacent centroids within the stent graft region.

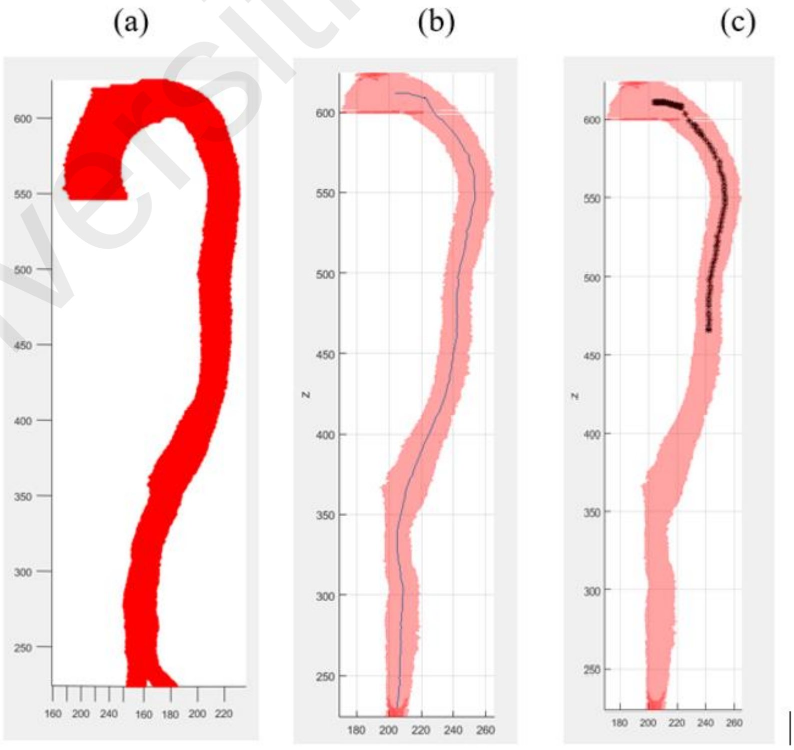

Figure 3-6 (a) Contour plot of aorta (b) plot of uniformly spaced centroid along the descending aorta (indicated by blue dotted line) (d) plot of centroids within the stent graft region

3.2 Overall workflow for structural finite element analysis

The overall workflow for structural simulation using the reconstructed patient-specific geometries and idealized models is shown in Figure 3.8.

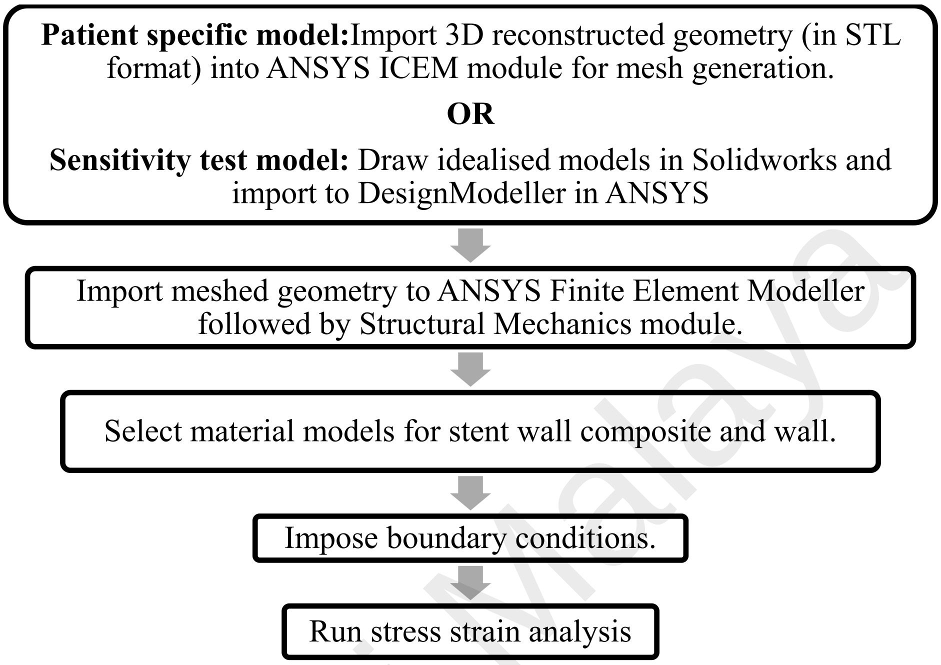

Figure 3-7 Overall workflow for structural finite element analysis.

3.2.1 Mesh generation

The 3D reconstructed geometry was imported into ANSYS ICEM module for mesh generation. Mesh sensitivity analysis was performed and a difference of less than 5% in the average equivalent stress (von Mises stress) between successive mesh sizes was deemed acceptable. Tetrahedral mesh was adopted for patient-specific models, while the hex dominant method with Quad/Tri free face mesh type was used for the idealised geometries. Tetrahedral mesh was adopted for the patient-specific models (with 2.1 – 3.1 million mesh elements and element sizes of 0.1 – 1.0 mm), while the hexahedral mesh was used for the idealised geometries (with 10876 to 12105 mesh elements).

3.2.1.1 Mesh dependency test

Mesh dependency test was performed for both patients and idealised models. Quadratic element setting was used (Element order =2). Patient with the highest STI/ inflection at the distal stent graft end (P3) was selected. Based on the results for P3 (Table 3.2), the maximum global element seed size of 0.7 units was applied on all patients as the difference in both stress and strain results with its consecutive mesh size (i.e. 0.66) is less than 5%. This resulted in mesh elements ranging between 2.1 to 3.1 million for all patients.

Table 3.2 Mesh dependency test results for Patient 3.

Max global element seed size (mm)	**0.66**	**0.7**	**0.8**	**0.9**
Mesh nodes	737404	222720	2036621	279818
Mesh elements	3625212	470154	429920	1278578
Von Mises stress (kPa)	490.5	490.43	490.36	771.77
% difference	0.0143	0.0143	-36.463	
Shear elastic strain	0.2245	0.22456	0.22457	0.2137
% difference	-0.0267	-0.0044	5.0865	
Displacement (mm)	6.2729	6.27351	6.27951	6.3552
% difference	-0.0097	-0.096	-1.191	

Based on the results for an idealised model (Table 3.3), the maximum face size of 1.9 units with a growth rate of 1.50 was applied on all idealised models. This resulted in mesh elements ranging between 10485 to 13655 for all idealised geometries.

Table 3.3 Mesh dependency results for an idealised model

Max face size (mm)	**1.7**	**1.8**	**1.9**	**2.0**
Mesh nodes	70577	63526	57636	52897
Mesh elements	13655	12099	11114	10485
Von Mises stress (kPa)	263.19	264.33	260.59	261.69
% difference	-0.43	1.44	-0.42	
Shear elastic strain	0.14691	0.14657	0.14632	0.14665
% difference	-0.23	-0.17	0.23	
Displacement (mm)	8.1242	8.1248	8.1292	8.1294
% difference	-0.01	-0.05	-0.002	

3.2.2 Material models

The composite stent-vessel wall region was described using the linear elastic material model with an elastic modulus of 8.4 MPa (Menichini et al., 2018), while the aortic wall was modelled as hyperelastic, using the 5-parameter Mooney-Rivlin constitutive equation. The strain energy density function of the hyperelastic model (adapted from (Tan, Mokhtraudin, Liew, Johari, & Lim, 2019)) was defined as follow:

$$W = C_{10}(\overline{I}_1 - 3) + C_{01}(\overline{I}_2 - 3) + C_{20}(\overline{I}_1 - 3)^2 + C_{11}(\overline{I}_2 - 3)(\overline{I}_2 - 3) + C_{02}(\overline{I}_2 - 3)^2 + \frac{1}{d}(J-1)^2 \qquad (3.3)$$

where $C_{10}, C_{01}, C_{20}, C_{11}, C_{02}$ $c_{10}, c_{01}, c_{20}, c_{11}, c_{02}, d$ are material constants, $\overline{I}_1$ and $\overline{I}_2$ are strain invariants and d is the incompressibility parameter (d=1x10^{-8}). The model parameters were determined by fitting experimental data of excised human aneurysmal abdominal aortic specimens (AAA) (Raghavan, Webster, & Vorp, 1996), , which were obtained from a group of human patients with mean age of 69 + 2 years. Due to the lack of experimental data characterizing material properties for AD tissue, data from AAA cases, which more closely resemble that of the AD patients as compared to the healthy tissue, was chosen. The optimized coefficients of the 5-parameter MR models are 0.50359, -0.43898, 0.63059, 0.013136 and 0.001291 in MPa. K = 2/d, where K is the bulk modulus. The bulk modulus was set to be 2 x 10^8 kPa to model the nearly incompressible behavior of the aorta.

3.2.3 Boundary conditions and simulation study

A static pressure of 50 mmHg was applied in a perpendicular direction to the inner surface, as it simulates the change in pressure in the aorta from diastole to systole (i.e. nominal pulse pressure). Since invasive aortic blood pressure measurements were unavailable in these patients, the same static pressure value was applied for all patients to enable a fair comparison. Fixed constraint was applied at the inlet, outlet and the side branches. Structural analysis was performed using the ANSYS Static Structural Solver (Version 19.0, Ansys Inc, Canonsburg, PA, USA). Equivalent stress (also known as von Mises stress), where the von Mises stress, shear elastic strain and displacement were analyzed. The displacement, D, at every nodal position in the finite element model (as produced by the inner wall pressure) was calculated as follows:

$$D = \sqrt{\Delta x^2 + \Delta y^2 + \Delta z^2} \tag{3.3}$$

where Δx , Δy and Δz are displacement vectors in the x ,y and z directions

3.3 Sensitivity study

In order to investigate the effect of several geometrical characteristics (reported to be potential risk factors for dSINE): (i) stent graft length; (ii) wedge apposition angle; and (iii) stent tortuosity on stent/strain distribution, sensitivity analysis was performed using idealised geometries of the aorta.

3.3.1 Generation of the idealised geometries

The centreline of the ideal aortic geometry was drawn as a combination of curves (curves 1 – 3 and a straight segment) with different radius of curvatures, which were determined based on Belvoy's study, 2019 (Belvroy et al., 2019), as shown in Figure 3.9. The inner radius of all models was fixed at 13.1 mm (i.e. average aortic radius of the patients) and the wall thickness was 1.4 mm. The same material model and boundary conditions, as that used in patient-specific simulation, were applied in the sensitivity study.

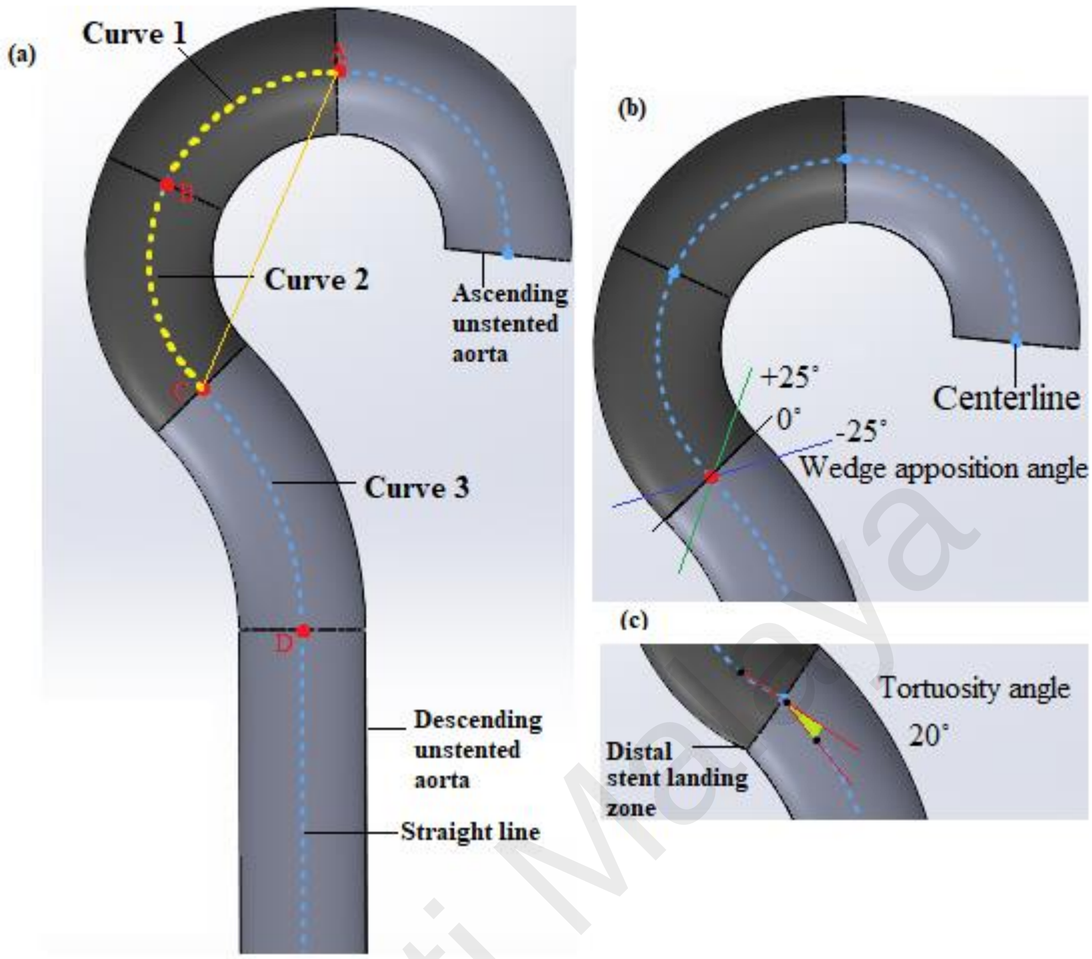

Figure 3-8 (a) Idealised aortic model with different curvatures along the aorta (b) variation of wedge apposition angle; and (c) variation of tortuosity angle at the distal stent-wall interface. Blue dashed line indicates the centerline of the aorta, dark grey region represents the stent graft region while light grey region represents the unstented region. (Curve 1: A to B, Curve 2: B to C, Curve 3: C to D).

3.3.2 Model variation

For stent graft length analysis, the proximal landing zone was fixed at the level after the left common carotid artery, covering the left subclavian artery, while six different models with different stent graft lengths (50, 80, 100, 130, 160, and 180 mm) were generated. The wedge apposition angle at both the proximal and distal landing end (i.e. stent graft end surface perpendicular to the aortic centreline) was set at 0^0.

Each of these models was then modified by rotating the distal stent graft end surface by 25˚ anti-clockwise (to simulate a distal wedge apposition angle of +25˚) and -25˚ clockwise (to simulate a distal wedge apposition angle of -25˚).

To investigate the effect of tortuosity angle at the distal stent-vessel interface, four models with different tortuosity angles (5˚, 10˚, 20˚ and 30˚) were reconstructed with a stent graft length of 100 mm and a distal wedge apposition angle of 0^0, by varying the vessel shape and length at the stented region. As tortuosity angle was varied, stent tortuosity index (STI) was also varied accordingly.

3.3.3 Inclusion of the intercostal arteries

To investigate the effect of side movement restrictions, ten pair of intercostal arteries were added to the four idealised models with different tortuosity angles (5˚, 10˚, 20˚ and 30˚). The intercostal arteries were equally spaced at an angle of 10˚ for all models. The diameter of each intercostal arteries was 2.2 mm, while the lengths of the intercostal arteries at the inner and outer curvature were set as 5.9 cm and 45.3 cm, respectively (Ma, Dong, Wang, et al., 2018). An example of the model was shown in Figure 3.10. Fixed constraints were applied at all ends of the intercostal arteries.

Figure 3-9 An example of an idealised model (tortuosity angle = 5º) with the inclusion of 10 pairs of intercostal arteries.

CHAPTER 4: RESULTS AND DISCUSSION

In the first section of this chapter, several geometrical measurements, which have been proposed as potential risk factors for dSINE, were presented for all patients. Next, results from the mesh dependency test, used for the selection of mesh sizes, were presented. Structural finite element analysis on all six selected patient geometries using the acute, hyperelastic material model, were then presented. Finally, sensitivity analysis results on the effect of stent graft length, wedge apposition angle and stent tortuosity on stress and strain distribution at the distal stent-vessel interface using idealised geometries were presented. In addition, simulation results on the effect of lateral intercostal artery support were presented. The last section of this chapter is the discussion.

4.1 Geometrical measurements

Table 4.1 shows the post TEVAR characteristics of all patients. The proximal (PD) and distal landing diameters (DD) of the stent graft showed high variations among subjects. With regards to taper ratio, P1 showed the highest taper ratio (TR), with a 41.8% reduction in diameter from the proximal to the distal stent graft end. In terms of stent tortuosity , P3 had significantly higher STI (i.e. 1.64) compared to other patients (i.e. 1.20 – 1.36). The high STI in this patient was accompanied by a substantially higher tortuosity angle (TA) at the distal stent-vessel interface (11.9 + 2.1 ˚). This was followed by P4, which had the second highest tortuosity angle at 8.18± 1.19˚, even though the STI was not substantially higher compared to other patients. With regards to stent graft length (SL), both P4 and P5 had longer stent graft length (i.e. 180 – 200 mm) compared to other patients, while P6 had the shortest stent graft length (i.e. 135 mm). Long and short stent length were observed in both group of patients.

Table 4.1 Post TEVAR characteristics of patients with and without dSINE. For each patient, 3 separate measurements were taken for tortuosity angle to account for the error.

Geometrical Parameters	dSINE patients			Non-dSINE patients		
	Patient 1	**Patient 2**	**Patient 3**	**Patient 4**	**Patient 5**	**Patient 6**
PD (mm)	31.1	28.8	33.2	27.5	32.3	28.8
DD (mm)	18.1	24.1	21.9	19.2	21.5	27.9
TR	0.42	0.16	0.34	0.30	0.33	0.03
STI	1.20	1.36	1.64	1.33	1.28	1.29
TA (˚)	4.9±1.2	5.8±1.3	11.9±2.1	8.18± 1.19	4.7±0.3	4.07±0.3
SL (mm)	150	140	200	180	200	135

4.2 Patient-specific simulations

Figure 4.1 compares the distribution of von Mises stress, shear elastic strain and displacement of dSINE (P1-3) and non-dSINE (P4-6) patients. Maximum von Mises stress was observed at the distal stent-vessel interface in all patients due to material mismatch, whereby the less stiff tissue exerts high pulling forces on the stent, resulting in high stress at the interface. However, P3 showed the highest value of von Mises stress (i.e. 490 kPa), which was located in the region where a large aneurysm was discovered at 14 months follow-up. This was followed by P2 and P5, which showed similar maximum von Mises stress values (248 and 247 respectively), followed by P6 (243 kPa). Meanwhile, P4 and P1 showed relatively low von Mises stress compared to other patients (i.e. 210 and 191 kPa, respectively). The high von Mises stress observed in P3 corresponded to their higher stent tortuosity (Table 4.1), which led to an increase in the displacement force at the middle of the stented region with a maximum aorta displacement of 6.3 mm (Figure 4.1), due to axial migration of the stent and thus elevated stress at the stent-vessel interface. While P2 and P3 experienced dSINE at follow up, no new tear was observed at the distal region in P5 and P6 despite the presence of high stress and displacement forces at the distal end of the stent graft.

The location of the new tear formation at the descending aorta region was found to coincide with the maximum shear elastic strain location for P2 and P3, but not for P1 (Figure 4.1). While P3 showed a significantly higher maximum von Mises stress value compared to other patients, the maximum shear elastic strain was only slightly higher , (i.e. 0.27). Despite the presence of low stress and strain, P1, who demonstrated substantially higher taper ratio than the other patients, showed new tear formation during follow up as a result of migration of the spring back stent graft as the aorta true lumen diameter restored. The high taper ratio could have led to excessive oversizing and radial force on the true lumen at the distal landing zone (Canaud et al., 2019), which could not be captured in the present study as the stent graft has not been modelled as a separate entity.

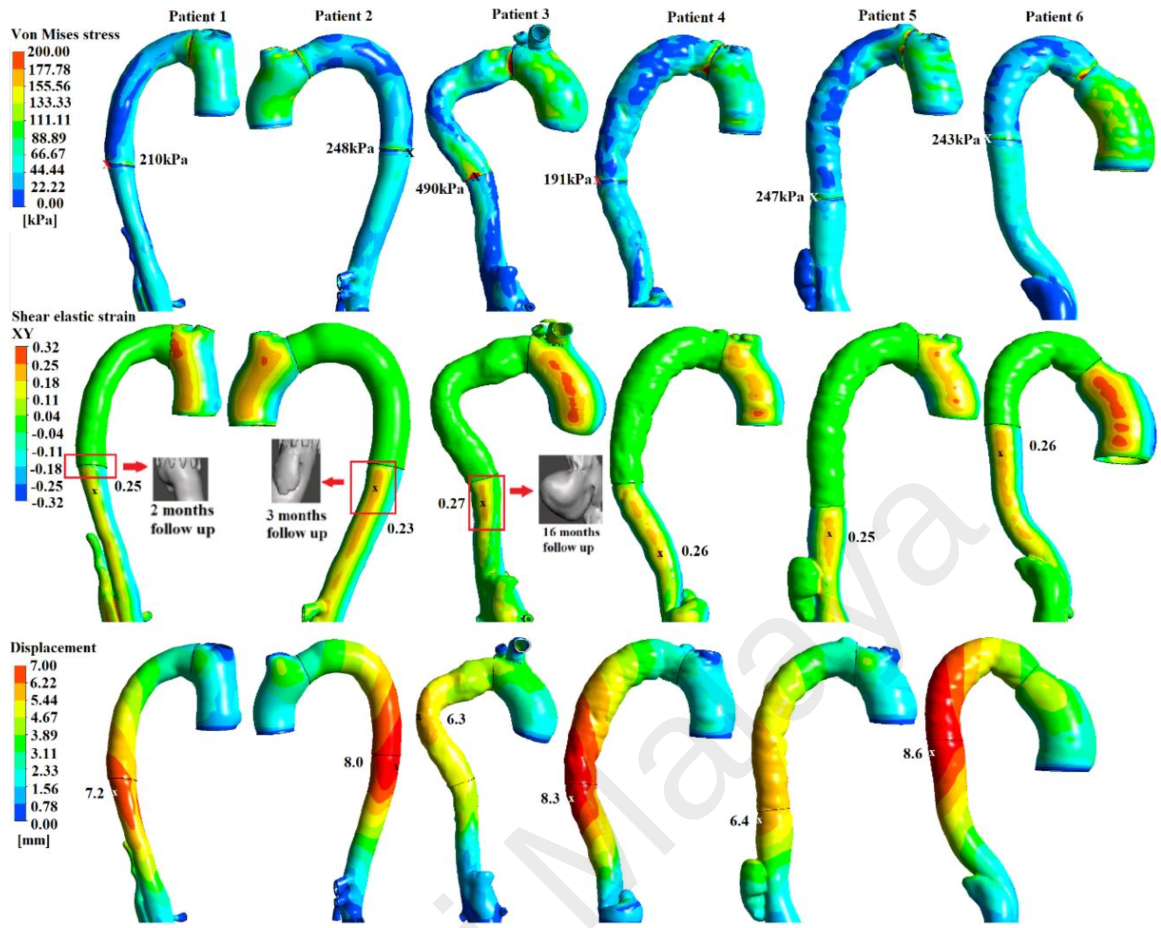

Figure 4-1 (a) Von Mises stress, (b) shear elastic strain and (c) displacement distribution for all patients. Locations with maximum values were marked with 'x', and their respective values were indicated next to 'x'. The location of new entry tear formed at follow up is indicated with red brackets for dSINE patients (patients 1-3)

4.3 Sensitivity analysis results

4.3.1 Effect of stent graft length

Figure 4.2 shows the effect of stent graft length variation on von Mises stress and shear elastic strain. As compared to stents 5-6 which landed at the straight aorta segment distally, stents 1-4, which landed along the curved segments demonstrated higher von Mises stress , (i.e. 245 – 342 kPa for stents 1 – 4 vs. 227 – 231 kPa for stents 5 – 6). Stent model 3, which had a distal landing zone at the plane with inflection point between curves 2 and 3, experienced the highest maximum von Mises stress (i.e. 342 kPa) among all. Overall, the maximum von Mises stress for stents 1-4 was located at the distal stent-vessel interface on the concave surface. For the straight segment (stents 5 – 6), the maximum von Mises stress is at the middle region.

With regards to shear elastic strain, stents models 1 – 3 demonstrated higher shear elastic strain compared to stents models 4 – 6 ,(i.e. 0.146 – 0.167 for stents 1 – 3 vs. 0.122 – 0.131 for stents 4 – 6). For stents models 1 – 3, the maximum strain was located at the concave surface near the plane with inflection point between curves 2 and 3 (Figure 4.2). When this region (with maximum strain) was covered by the stent, as observed in stents models 4 – 6, substantial drop in the maximum shear elastic strain occurred, and its location shifted to the distal stent-vessel interface.

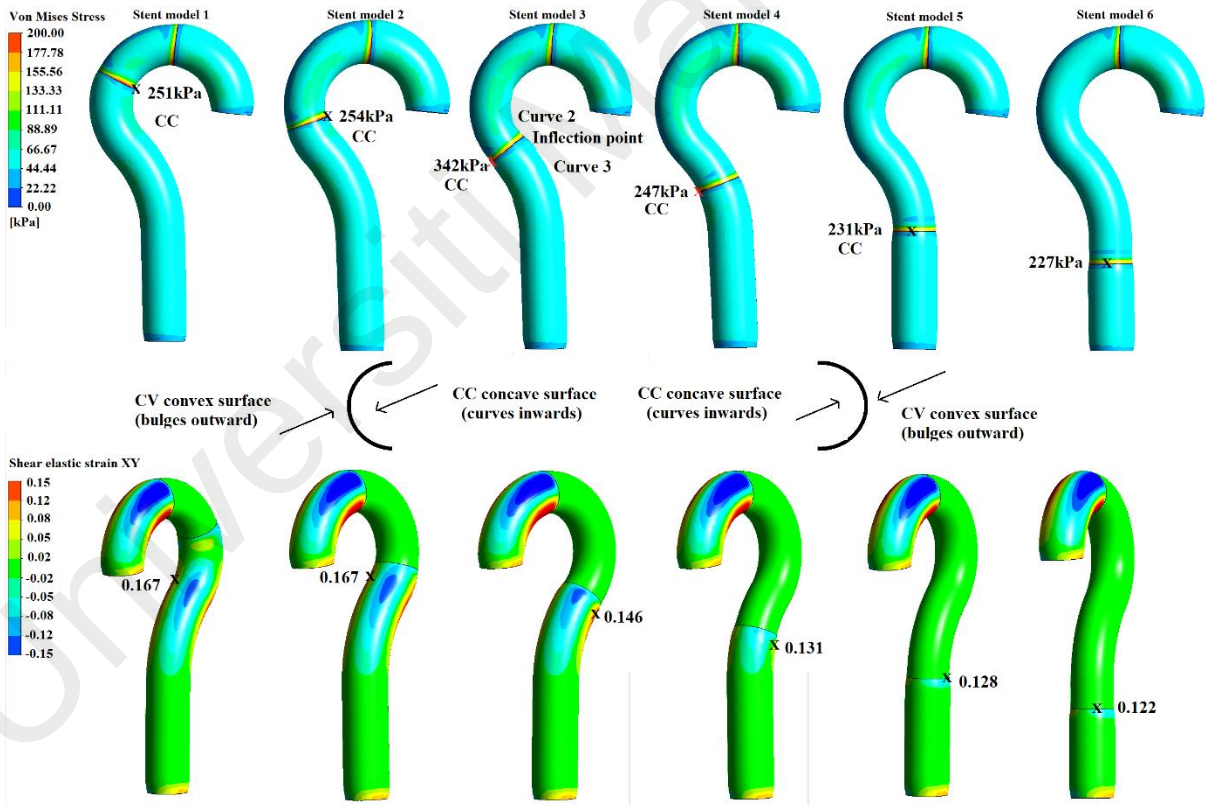

Figure 4-2 Von Mises stress and shear elastic strain distribution for different stent graft lengths (Stent model 1: 50mm, Stent model 2: 80mm, Stent model 3: 100mm, Stent model 4: 130mm, Stent model 5: 160mm, Stent model 6: 180mm). Locations with maximum values were marked with 'x', and their respective values were indicated next to 'x'. Higher value was observed when the maximum von Mises stress occurred at the concave (CV) surface compared to the convex (CC) surface.

4.3.2 Effect of distal wedge apposition angle

Figure 4.3 shows that the location of the maximum von Mises stress remained predominantly at the concave region of the aorta despite a change in the distal wedge apposition angle (from 0 ˚ to either +25 ˚ or -25 ˚). For the short stent models with distal stent graft end landing at the high curvature region (stents 1 – 2), the magnitude of von Mises stress increased with a +25 ˚ shift in the distal wedge apposition angle (Figure 4.4). Meanwhile, opposite phenomenon (i.e. a reduction in the maximum von Mises stress) was observed with a -25 ˚ shift in the distal wedge opposition angle. On the other hand, stent model 3, which experienced the highest maximum von Mises stress among all at baseline, demonstrated a substantial reduction in the magnitude of von Mises stress with a change in the distal wedge apposition angle from 0 ˚ to either +25 ˚ or -25 ˚.

While transitioning into the straight aortic segment (stent models 4), an increase in the maximum von Mises stress was observed with a -25 ˚ distal wedge apposition angle. Stent model 5, which had its distal landing zone at the straight segment, showed an increase in the maximum von Mises stress for both configurations compared to the original model. The tilting of the distal stent graft end plane caused one side of the distal stent graft to land on the straight aorta segment (i.e. outer curvature for +25 ˚ and inner curvature for -25 ˚), and another side on the curved aorta segment. On the other hand, maximum von Mises stress for stent model 6 remained relatively unchanged regardless of the tilting configurations as the distal stent graft landed at the straight aorta segment.

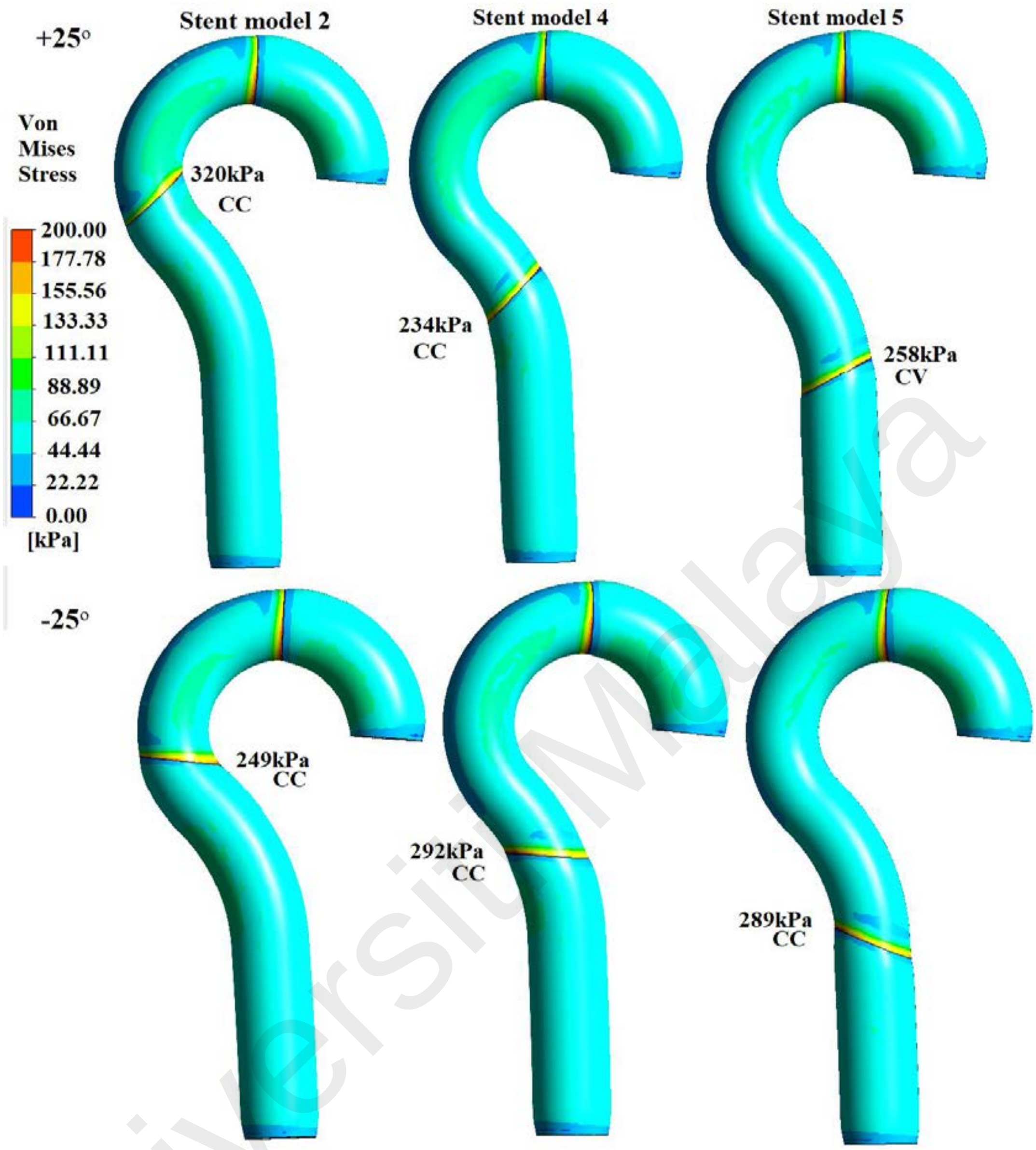

Figure 4-3 Von Mises stress distribution for stent models 2, 4 and 5 at +25˚ and -25˚ distal wedge apposition angle. CC: concave surface, CV: convex surface

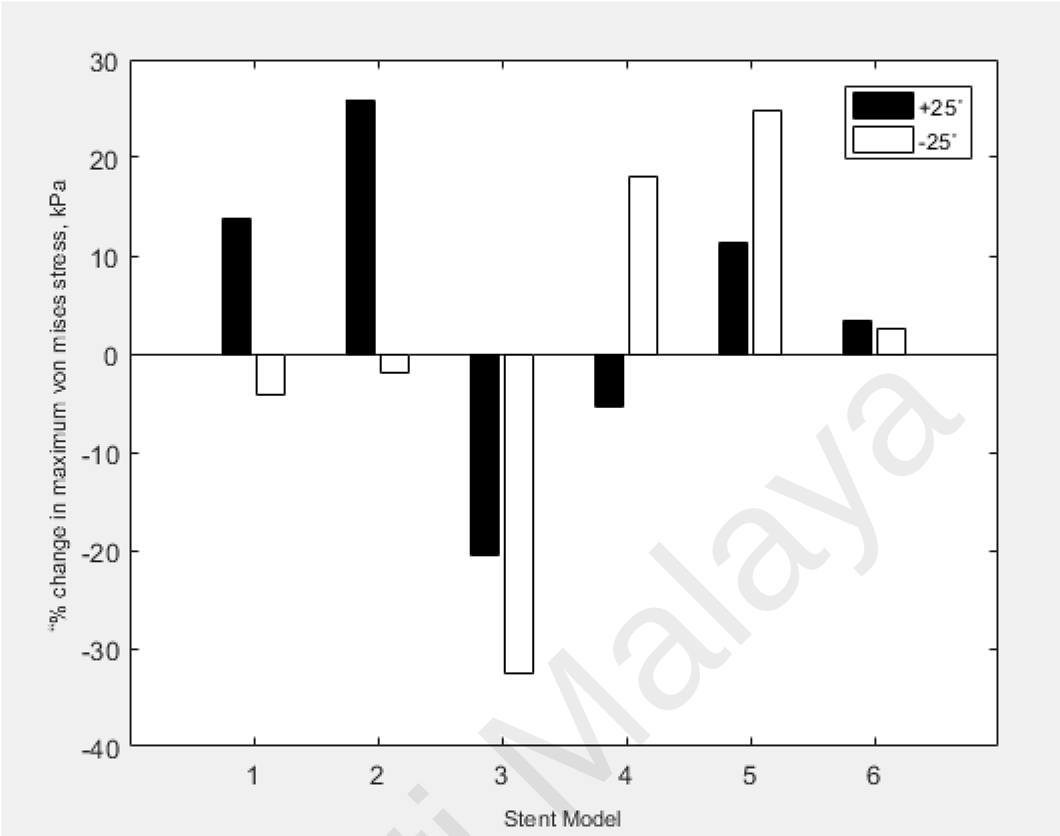

Figure 4-4 Percentage change in the maximum von Mises stress at 25˚ and -25˚ distal wedge apposition angle when compared to 0 ˚

4.3.3 Effect of stent tortuosity (inclusion /exclusion of intercostal arteries)

As stent tortuosity increased, an increase in the displacement magnitude and shear elastic strain was observed (Table 4.6), leading to an increase in the maximum von Mises stress at the distal stent-vessel interface (from 263.3 kPa with a 5˚ tortuosity angle to 312.9 kPa with a 30˚ tortuosity angle) (Figure 4.5 and Table 4.2).

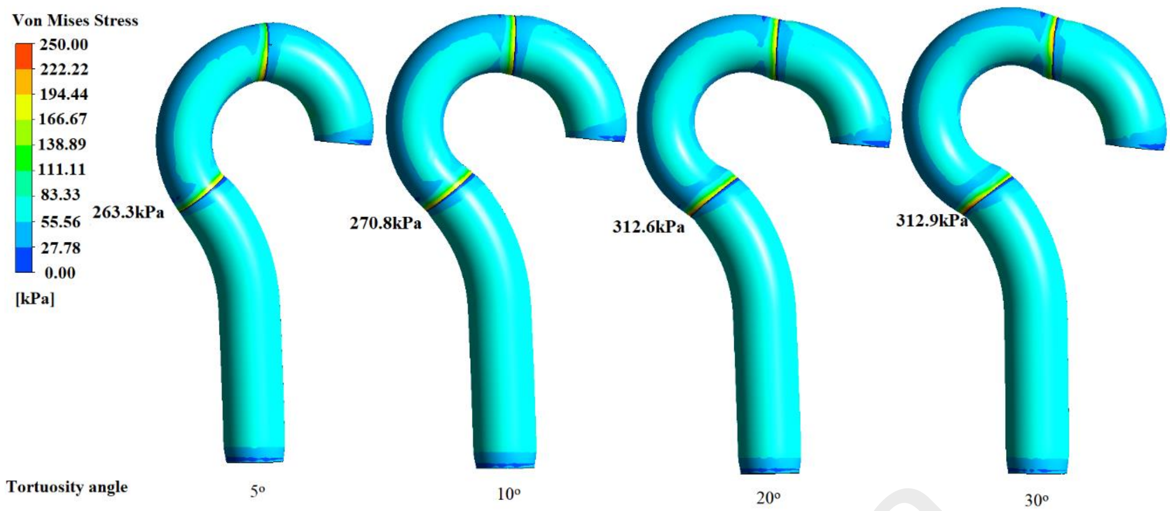

Figure 4-5 Von Mises stress contours for models with different tortuosity angles at the distal stent-vessel interface.

Table 4.2 Maximum von Mises stress and shear elastic strain of the aorta with variations in the tortuosity angles (TA) at the distal stent-vessel interface/ stent tortuosity index (STI) with (WLS) and without lateral support (WOLS).

TA [˚]	STI	Von Mises stress [kPa]		% diff	Shear elastic strain		% diff	Displacement
		WLS	WOLS		WLS	WOLS		WOLS
5	1.20	256.88	263.33	2.45	0.138	0.146	5.48	8.13
10	1.38	270.34	270.79	0.165	0.139	0.148	6.08	8.23
20	1.57	301.86	312.61	3.44	0.146	0.153	4.58	8.70
30	1.72	310.84	312.92	0.66	0.147	0.155	5.16	9.07

As observed in Figure 4.6, the displacement of the stented region was reduced due to movement restriction imposed by the lateral support, at an expense of a reduction in the displacement of the distal unstented region. However, the effect of lateral support on the stress and strain distribution was negligible. Table 4.2 showed that despite an inclusion of the lateral support by the intercostal arteries, the von Mises stress and shear strain at the distal interface remained its increasing trend with an increase in stent tortuosity. The presence of side branches in the model restricts aortic displacement of the stent wall composite, which reduced the straining of the aorta around the stent-graft region and led to a reduction in the maximum von Mises stress at the distal stent end. However, the overall trend of the results, in terms of changes in stress/strain with STI, remained relatively unchanged.

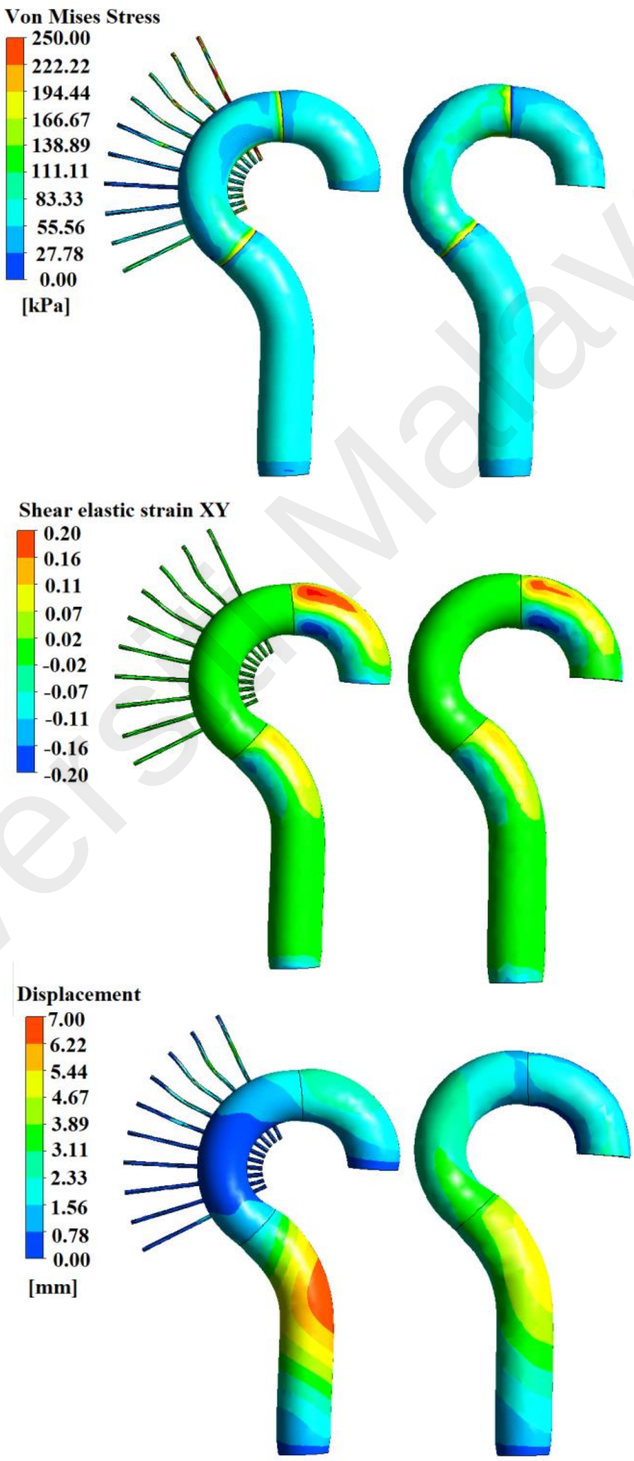

Figure 4-6 Comparison of von Mises stress, shear elastic strain and displacement distribution with and without the inclusion of intercostal arteries, using idealised models at a 10° tortuosity angle.

4.4 Discussion

Due to the existence of various confounding factors in clinical studies and huge variation in patients' anatomy, to date, contradictory findings have been reported with regards to the risk factors for dSINE. These include distal stent graft oversizing (Canaud et al., 2019; C.-Y. Huang et al., 2016; Jánosi et al., 2015; Lescan et al., 2019; Ma, Dong, Fu, et al., 2018; Pantaleo et al., 2016; Weng et al., 2013; Zhao et al., 2018), tapering ratio (C.-Y. Huang et al., 2016; Jang et al., 2017; Jánosi et al., 2015; Lescan et al., 2019; Weng et al., 2013), age of dissection (Jánosi et al., 2015; Theodorus MJ van Bakel et al., 2018), stent graft length (Jánosi et al., 2015; Lescan et al., 2019; Q. Li et al., 2019; Q. Li et al., 2015; Ma, Dong, Fu, et al., 2018; T. M. van Bakel et al., 2018) and vessel curvature (Menichini et al., 2018; Spinella et al., 2018). For instance, while Lescan et al. 2019 (Lescan et al., 2019) and Li et al. 2015 (Q. Li et al., 2015) found that patients with dSINE had a shorter stent graft length (< 145 mm) compared to those without dSINE, Janosi et al., 2015 (Jánosi et al., 2015) observed no significant difference in stent graft length between these two cohorts. In order to address this, the present study has provided detailed biomechanical analysis on the effect of key anatomical characteristics, namely stent graft length, distal wedge apposition angle and stent tortuosity, on important biomechanical variables (i.e. stress, strain and displacement force), which could lead to the formation of dSINE.

The patient-specific simulation results showed maximum von Mises stress at the distal stent vessel interface in all patients, with maximum shear elastic strain occurring at the neighbouring distal region, except for P1 (Figure 4.1). This was attributed to the mismatch in biomechanical properties between the stented and the nonstented regions. Consistent with previously published findings (Chen et al., 2018; Menichini et al., 2018), excessively high tortuosity, as that observed in P3, was a risk factor for the occurrence of dSINE, as it substantially elevated maximum von Mises stress at the stent-vessel interface. Meanwhile, other patients in this study demonstrated comparable stress/strain, regardless of the occurrence of dSINE. Compared to P3 which experienced excessive bulging/aneurysm at the new tear region during follow up, the occurrence of dSINE in P1 and P2 was much less severe with no obvious occurrence of aneurysm. The main contributor of dSINE risk in P1 is believed to be partly due to the high taper ratio of the aorta (Weng et al., 2013), as the stent graft migrated due to high spring back force of the stent graft at the distal stent graft edge. The taper ratio between the proximal and distal landing zones in pre-TEVAR has been reported to be higher in the dSINE compared to non-dSINE groups (Jang et al., 2017). For P1, the tapering in pre-TEVAR was about 14.6mm, whereas the maximum tapering of commercial stent graft is only 4mm. This indicates excessive oversizing at the narrower segment of the aorta when the stent graft is deployed in P1. Excessive oversizing exerts high radial force onto the aortic wall, increasing the risk of tearing and therefore triggering the development of dSINE. Although it is suspected that high taper ratio is a contributing risk factor for dSINE in P1, further simulation which incorporates a physical stent graft in the model is required to confirm this hypothesis.

The simulation results further showed no direct correlation between stent graft length and stress/strain magnitude or the formation of dSINE (Table 4.1, Figure 4.1). As stent graft (proximal end), anchored at the aortic arch, has the tendency to spring back to its straight status, it imposed a spring back force on the vessel wall, which may play a role in the occurrence of dSINE. Previous study has therefore suggested that shorter stent graft imposes a higher risk for dSINE formation due to the presence of a stronger spring-back force at the distal end of the stent graft (Qing Li et al., 2015). Nevertheless, in this study, despite having the shortest stent graft length, P6 experienced no higher von Mises stress compared to other patients, which could be explained by the fact that the stent graft landed at a relatively straight vessel region (low tortuosity angle) and the stent graft tortuosity is not high in this patient. P3 with longest stent graft length (200mm) experience high stress due to the presence of high stent tortuosity and distal stent landing at region with high curvature (high tortuosity angle). The sensitivity analysis results on stent graft length further revealed that stent graft tortuosity and wall curvature at the distal stent graft end plays an important role on stress/strain, where stent graft landing along the curved segments demonstrated significantly higher maximum von Mises stress and shear elastic strain compared to the straight segment (Figure 4.2). The present findings coincide with previously published computational study on abdominal aortic aneurysm (AAA) (Elger, Blackketter, Budwig, & Johansen, 1996),which highlighted that AAA wall curvature (instead of bulge diameter) is correlated with maximum stress, and therefore could better predict the risk of AAA rupture. The present results also showed that the stress/strain magnitude was further amplified by stent graft landing at the inflection point of a curve. One notable finding in this study was that the position of the maximum von Mises stress for stent graft models landing along the curved segment fell on the concave surface at the distal stent-vessel interface, as this region experienced a larger amount of compressive force compared to the convex surface.

While a few previously published studies (Figueroa, Taylor, Chiou, Yeh, & Zarins, 2009; Ma, Dong, Fu, et al., 2018; Menichini et al., 2018) have demonstrated an increase in wall stress when stent graft was deployed in a tortuous geometric plane, they were based on very limited number of patient geometries with substantial variations in anatomical characteristics other than stent graft tortuosity. In this study, in addition to using patient-specific simulations, sensitivity analysis was performed to independently assess the effect of stent graft tortuosity on key biomechanical variables using fixed proximal and distal landings. Stent graft tortuosity was quantified both globally (using

STI) and regionally (using tortuosity angle at the distal stent-vessel interface). Increase in stent graft tortuosity caused an increase in the displacement at the stented region and von Mises stress at the distal stent-vessel interface, which in turn led to an increasing risk of dSINE formation (Table 4.2).

With regards to the wedge apposition angle, the simulation results showed that a change in the distal wedge apposition angle by +25˚ at a fixed stent graft tortuosity could substantially vary the maximum von Mises stress. Generally, the location of the maximum von Mises stress remained predominantly on the concave surface. When this region coincides with the surface with reduced distance between the distal stent graft end and the proximal stent graft end upon tilting of the distal stent graft plane (e.g. +25˚ for stent model 2 and -25˚ for stent models 5), a substantial increase in the maximum von Mises stress was observed (Figures 4.3 and 4.4). This could be explained by a greater wall expansion of the unstented region on this surface. Interestingly, a substantial reduction in the magnitude of von Mises stress was observed with a deviation of the distal wedge apposition angle from 0º for stent model 3, which experienced the highest maximum von Mises stress among all at baseline (i.e. 0 ˚) (Figure 4.4). The slanted distal stent graft edge creates an asymmetrical segment within the aorta, which expands unevenly upon application of an internal pressure to the aortic wall. On the contrary, wedge apposition angle has minimal effect on the maximum von Mises stress when the distal stent graft landed at the straight aorta segment (stent 6). The present simulation results highlighted the importance of distal wedge apposition angle in determining wall stress, and may explain a recent clinical finding by Lescan et al., 2019 (Lescan et al., 2019), which identified the wedge apposition angle as the most significant risk factor for dSINE, ahead of stent graft length and taper ratio.

CHAPTER 5: CONCLUSION

5.1 Conclusions

Type B AD patients with severe dSINE have high STI and high tortuosity angle at the distal stent-grant end as compared to non dSINE patients. High maximum equivalent stress at the distal edge of the stent-wall composite potentially indicates the presence of stent graft induced straining effect due to material mismatch. The material mismatch of the aorta has resulted in concentrated stress region due to the interaction of the material wall with the implanted stent graft. Distal stent graft landing at highly tortuous vessel region (high STI, tortuosity angle), in particular at the inflection point of a curve, led to high von Mises stress at the distal stent-vessel interface, which could induce dSINE. Malapposition of the aorta (as reflected by different wedge apposition angles) created an asymmetrical segment within the aorta, thus varying the location and magnitude of the maximum von Mises stress. Increase in stress was observed at the concave surface of the aorta where the maximum von Mises stress occurred. In this study, it is observed that stent tortuosity and wedge apposition angle are major risk factors for the formation of dSINE in AD patients regardless of stent graft length.

Thus, selection of stent graft length should be tailored to patient-specific geometry, so that the deployed distal stent graft edge is positioned at a straighter portion of the aorta. It can be concluded from this work that stent tortuosity and wedge apposition angle are major risk factors for the formation of dSINE in AD patients. Recent treatment technique by inserting stent graft through the distal region rather than the conventional proximal region is expected to produce safer outcomes as the size of the aorta could be more accurately estimated to avoid the issue of distal oversizing and the error of placing the stent graft edge at the inflection point can be prevented. Thus, the recommend selection of stent graft length should be tailored to patient-specific geometry, so that the deployed distal stent graft edge is positioned at a straighter portion of the aorta.

5.2 Limitations and future work

The goal of this work is to study the biomechanical effects (in terms of stress and strain) of stent graft placement in dissected aorta with different tortuosities, as well as at different stent graft lengths and distal wedge apposition angles. However, it is worth noting that as prediction of the aortic wall deformation due to stent graft deployment is not the focus of this work, post-operative geometry was utilized, and an ideal seal of the stent graft onto the aorta wall surface was assumed. Therefore, all simulation results presented in this work only captured the effect caused by a mismatch in material properties between the stent graft and the vessel wall in the presence of complex anatomical variations in AD patients. Future work should consider modelling the deployment of an actual stent graft into the aorta.

In the present work, static CT scan images, which involved only one-time point of patient geometry acquisition, were acquired from retrospective studies. Information about the distention of the aorta throughout the cardiac cycle was unavailable, and thus it cannot be confirmed that the maximum diameter of the vessel CT images are used for image reconstruction. Future work may consider using dynamic scans such as MRI for acquiring more detailed geometrical information.

In addition, several anatomical simplifications and assumptions were made. Owing to the lack of data availability, cohort-averaged values based on published literature have been used for the vessel wall material parameters and wall thickness, and the changes in material properties over time due to tissue growth and remodelling were not taken into account. Aorta wall thickness was not extracted directly from CT images due to the thin wall structure and insufficient system resolution. This limitation has also been reported in published clinical and simulation studies (B. J. Doyle et al., 2008; Mao et al., 2008; Martufi, Di Martino, Amon, Muluk, & Finol, 2009; Miller et al., 2020; Venkatasubramaniam et al., 2004). In addition, the dissected aorta was assumed to be under zero residual stress state, as calculation of the residual stress involves complicated nonlinear material analysis. Therefore, the absolute wall stresses and strains presented in the current study do not represent the actual values. However, the major outcomes of this study, which involve the trend of the maximum von Mises stress with anatomical variations, should still follow. Future work may also consider performing dynamic simulation, which takes into account fatigue of the aorta structure.

Furthermore, external tissue support and side branches were not included in the model, which may restrict aortic displacement. Nevertheless, due to the relatively stiff material properties of the stent graft, the effect of the surrounding environment onto the vessel surface is minimal. More importantly, our further analysis as shown in Section 4.3.3 , showed that the increasing trend of stress and strain values at the distal stent-vessel interface with increasing vessel tortuosity remain unchanged with the addition of the intercostal arteries to provide external support. Fluid simulation and fluid structure interaction were also not considered in this study.

Material models implemented in the literature for AD simulation studies were mainly derived from either animal sources or surgical specimens of patients with vessel diseases. Characterization of material properties for AD patients using experimental studies are currently lacking. However, the material models applied in this study were believed to be within the realistic range of aortic stiffness for diseased aorta.

Finally, only a small number (N = 6) of patients were included in this study. Future studies using a larger sample size are needed to further strengthen the findings. The current patient-specific simulation study was also limited by considering the geometry at a single time point (i.e. at post-TEVAR). Changes of the geometry over time is possible after stent graft implantation, which may be worth studying in the future.

REFERENCES

Ahmadzadeh, H., Rausch, M., & Humphrey, J. (2018). Particle-based computational modelling of arterial disease. *Journal of The Royal Society Interface, 15*(149), 20180616. doi:https://doi.org/10.1098/rsif.2018.0616

Ahuja, A., Guo, X., Noblet, J. N., Krieger, J. F., Roeder, B., Haulon, S., . . . Kassab, G. S. (2018). Validated Computational Model to Compute Re-apposition Pressures for Treating Type-B Aortic Dissections. *Frontiers in Physiology, 9*(513). doi:10.3389/fphys.2018.00513

Aoyama, T., Kunisawa, S., Fushimi, K., Sawa, T., & Imanaka, Y. (2018). Comparison of surgical and conservative treatment outcomes for type a aortic dissection in elderly patients. *Journal of Cardiothoracic Surgery, 13*(1), 129. doi:10.1186/s13019-018-0814-6

Belvroy, V. M., De Beaufort, H. W., Van Herwaarden, J. A., Bismuth, J., Moll, F. L., & Trimarchi, S. (2019). Tortuosity of the descending thoracic aorta: Normal values by age. *PloS one, 14*(4), e0215549. doi: 10.1371/journal.pone.0215549

Booher, A. M., Isselbacher, E. M., Nienaber, C. A., Trimarchi, S., Evangelista, A., Montgomery, D. G., . . . Januzzi, J. L. (2013). The IRAD classification system for characterizing survival after aortic dissection. *The American Journal of Medicine, 126*(8), 730. e719-730. e724. doi: 10.1016/j.amjmed.2013.01.020.

Brown, A. G., Shi, Y., Marzo, A., Staicu, C., Valverde, I., Beerbaum, P., . . . Hose, D. R. (2012). Accuracy vs. computational time: translating aortic simulations to the clinic. *Journal of Biomechanics, 45*(3), 516-523. doi: 10.1016/j.jbiomech.2011.11.041

Canaud, L., Gandet, T., Sfeir, J., Ozdemir, B. A., Solovei, L., & Alric, P. (2019). Risk factors for distal stent graft-induced new entry tear after endovascular repair of thoracic aortic dissection. *Journal of Vascular Surgery*. 69(5):1610-1614. doi: 10.1016/j.jvs.2018.07.086

Chen, D., Wei, J., Deng, Y., Xu, H., Li, Z., Meng, H., . . . Yan, T. (2018). Virtual stenting with simplex mesh and mechanical contact analysis for real-time planning of thoracic endovascular aortic repair. *Theranostics, 8*(20), 5758. doi: 10.7150/thno.28944

Cikach, F. S., Koch, C. D., Mead, T. J., Galatioto, J., Willard, B. B., Emerton, K. B., . . . Roselli, E. E. (2018). Massive aggrecan and versican accumulation in thoracic aortic aneurysm and dissection. *JCI insight, 3*(5). doi: 10.1172/jci.insight.97167

Dake, M. D., Thompson, M., van Sambeek, M., Vermassen, F., & Morales, J. P. (2013). DISSECT: A New Mnemonic-based Approach to the Categorization of Aortic Dissection. *European Journal of Vascular and Endovascular Surgery, 46*(2), 175-190. doi:https://doi.org/10.1016/j.ejvs.2013.04.029

de Beaufort, H. W., Ferrara, A., Conti, M., Moll, F. L., van Herwaarden, J. A., Figueroa, C. A., . . . Trimarchi, S. (2018). Comparative Analysis of Porcine and Human

Thoracic Aortic Stiffness. *European Journal of Vascular and Endovascular Surgery*. doi: 10.1016/j.ejvs.2017.12.014

Dong, Z., Fu, W., Wang, Y., Wang, C., Yan, Z., Guo, D., . . . Chen, B. (2010). Stent graft-induced new entry after endovascular repair for Stanford type B aortic dissection. *Journal of Vascular Surgery, 52*(6), 1450-1457.

Doyle, B. J., Morris, L. G., Callanan, A., Kelly, P., Vorp, D. A., & McGloughlin, T. M. (2008). 3D Reconstruction and Manufacture of Real Abdominal Aortic Aneurysms: From CT Scan to Silicone Model. *Journal of Biomechanical Engineering, 130*(3). doi:10.1115/1.2907765

Doyle, B. J., & Norman, P. E. (2016). Computational Biomechanics in Thoracic Aortic Dissection: Today's Approaches and Tomorrow's Opportunities. *Annals of Biomedical engineering, 44*(1), 71-83. doi:10.1007/s10439-015-1366-8

Elger, D., Blackketter, D., Budwig, R., & Johansen, K. (1996). The influence of shape on the stresses in model abdominal aortic aneurysms. J Biomech Eng, 118(3):326-32. doi: 10.1115/1.2796014

Erbel, R., Aboyans, V., Boileau, C., Bossone, E., Di Bartolomeo, R., Eggebrecht, H., . . . Gaemperli, O. (2014). 2014 ESC Guidelines on the diagnosis and treatment of aortic diseases. *Kardiologia Polska (Polish Heart Journal), 72*(12), 1169-1252. doi: 10.5603/KP.2014.0225

Fanelli, F., Cannavale, A., O'Sullivan, G. J., Gazzetti, M., Cirelli, C., Lucatelli, P., . . . Catalano, C. (2016). Endovascular Repair of Acute and Chronic Aortic Type B Dissections: Main Factors Affecting Aortic Remodeling and Clinical Outcome. *JACC: Cardiovascular Interventions, 9*(2), 183-191. doi:https://doi.org/10.1016/j.jcin.2015.10.027

Faure, E. M., Canaud, L., Agostini, C., Shaub, R., Böge, G., Marty-ané, C., & Alric, P. (2014). Reintervention after thoracic endovascular aortic repair of complicated aortic dissection. *Journal of Vascular Surgery, 59*(2), 327-333. doi: 10.1016/j.jvs.2013.08.089

Figueroa, C. A., Taylor, C. A., Chiou, A. J., Yeh, V., & Zarins, C. K. (2009). Magnitude and direction of pulsatile displacement forces acting on thoracic aortic endografts. *Journal of Endovascular Therapy, 16*(3), 350-358. doi: 10.1583/09-2738.1

Gao, F., Guo, Z., Sakamoto, M., & Matsuzawa, T. (2006). Fluid-structure interaction within a layered aortic arch model. *J Biol Phys, 32*(5), 435-454. doi:10.1007/s10867-006-9027-7

Gao, F., Watanabe, M., & Matsuzawa, T. (2006). Stress analysis in a layered aortic arch model under pulsatile blood flow. *Biomed Eng Online, 5*, 25. doi:10.1186/1475-925X-5-25

García-Herrera, C. M., Celentano, D. J., Cruchaga, M. A., Rojo, F. J., Atienza, J. M., Guinea, G. V., & Goicolea, J. M. (2012). Mechanical characterisation of the human thoracic descending aorta: experiments and modelling. *Computer Methods* *in Biomechanics and Biomedical Engineering, 15*(2), 185-193. doi: https://doi.org/10.1080/10255842.2010.520704

Giannakoulas, G., Giannoglou, G., Soulis, J., Farmakis, T., Papadopoulou, S., Parcharidis, G., & Louridas, G. (2005). A computational model to predict aortic wall stresses in patients with systolic arterial hypertension. *Medical Hypotheses, 65*(6), 1191-1195. doi:10.1016/j.mehy.2005.06.017

Grande, W., & Stavropoulos, S. W. (2006). Treatment of complications following endovascular repair of abdominal aortic aneurysms. *Seminars in interventional Radiology, 23*(2), 156-164. doi:10.1055/s-2006-941446

Haskett, D., Johnson, G., Zhou, A., Utzinger, U., & Geest, J. V. (2010). Microstructural and biomechanical alterations of the human aorta as a function of age and location. *Biomechanics and Modeling in Mechanobiology, 9*(6), 725-736. doi: 10.1007/s10237-010-0209-7

Huang, C.-Y., Chen, C.-W., Chen, P.-L., Chen, W.-Y., Chen, I.-M., Hsu, C.-P., & Shih, C.-C. (2016). Association between aortic remodeling and stent graft-induced new entry in extensive residual type A dissecting aortic aneurysm after hybrid arch repair. *Annals of Vascular Surgery, 31*, 60-69. doi: 10.1016/j.avsg.2015.08.022

Huang, C. Y., Weng, S. H., Weng, C. F., Chen, W. Y., Chen, I. M., Hsu, C. P., & Shih, C. C. (2013). Factors predictive of distal stent graft-induced new entry after hybrid arch elephant trunk repair with stainless steel-based device in aortic dissection. *J Thorac Cardiovasc Surg, 146*(3), 623-630. doi:10.1016/j.jtcvs.2012.07.052

Hughes, G. C. (2019). Stent graft–induced new entry tear (SINE): Intentional and NOT. *The Journal of Thoracic and Cardiovascular Surgery, 157*(1), 101-106. e103. doi: 10.1016/j.jtcvs.2018.10.060

Investigators, V. R. (2014). Mid-term outcomes and aortic remodelling after thoracic endovascular repair for acute, subacute, and chronic aortic dissection: the VIRTUE Registry. *European Journal of Vascular and Endovascular Surgery, 48*(4), 363-371. doi: 10.1016/j.ejvs.2014.05.007

Jang, H., Kim, M.-D., Kim, G. M., Won, J. Y., Ko, Y.-G., Choi, D., . . . Lee, D. Y. (2017). Risk factors for stent graft-induced new entry after thoracic endovascular aortic repair for Stanford type B aortic dissection. *Journal of Vascular Surgery, 65*(3), 676-685. doi: 10.1016/j.jvs.2016.09.022

Jánosi, R. A., Tsagakis, K., Bettin, M., Kahlert, P., Horacek, M., Al‐Rashid, F., . . . Erbel, R. (2015). Thoracic aortic aneurysm expansion due to late distal stent graft‐induced new entry. *Catheterization and Cardiovascular Interventions, 85*(2), E43-E53. https://doi.org/10.1002/ccd.25614

Kawatani, Y., Hayashi, Y., Ito, Y., Kurobe, H., Nakamura, Y., Suda, Y., & Hori, T. (2015). Treatment with Aortic Stent Graft Placement for Stanford B-Type Aortic Dissection in a Patient with an Aberrant Right Subclavian Artery. *Case reports in Vascular Medicine, 2015*, 746354-746354. doi:10.1155/2015/746354

Lescan, M., Czerny, M., Berezowski, M., Andic, M., Bamberg, F., Beyersdorf, F., . . . Rylski, B. (2019). Morphologic performance analysis of the Relay nonbare stent graft in dissected thoracic aorta. *Journal of Vascular Surgery*. doi:10.1016/j.jvs.2019.02.026

Li, D.-l., Zhang, H.-k., Chen, X.-d., Tian, L., Jin, W., & Li, M. (2016). Thoracic Endovascular Aortic Repair for Type B Aortic Dissection: Analysis Among Acute, Subacute, and Chronic Patients. *Journal of the American College of Cardiology, 67*(10), 1255-1257. doi:https://doi.org/10.1016/j.jacc.2015.12.044

Li, Q., Ma, W.-G., Zheng, J., Xu, S.-D., Chen, Y., Liu, Y.-M., . . . Sun, L.-Z. (2019). Distal Stent Graft-Induced New Entry After TEVAR of Type B Aortic Dissection: Experience in 15 Years. *The Annals of Thoracic Surgery, 107*(3), 718-724. doi: 10.1016/j.athoracsur.2018.09.043

Li, Q., Wang, L. F., Ma, W. G., Xu, S. D., Zheng, J., Xing, X. Y., . . . Sun, L. Z. (2015). Risk factors for distal stent graft-induced new entry following endovascular repair of type B aortic dissection. *Journal of Thoracic Disease, 7*(11), 1907-1916. doi:10.3978/j.issn.2072-1439.2015.11.27

Li, Z., & Kleinstreuer, C. (2005). Blood flow and structure interactions in a stented abdominal aortic aneurysm model. *Medical Engineering & Physics, 27*(5), 369-382. doi:https://doi.org/10.1016/j.medengphy.2004.12.003

Li, Z., & Kleinstreuer, C. (2007). A comparison between different asymmetric abdominal aortic aneurysm morphologies employing computational fluid–structure interaction analysis. *European Journal of Mechanics-B/Fluids, 26*(5), 615-631. doi: https://doi.org/10.1016/j.euromechflu.2007.03.003

Lu, T., Chen, Z., Qi, H. J., & Wang, T. (2018). A micro-structure based constitutive model for anisotropic stress–strain behaviors of artery tissues. *International Journal of Solids and Structures*. doi:https://doi.org/10.1016/j.ijsolstr.2018.01.025

Ma, T., Dong, Z. H., Fu, W. G., Xu, X., Chen, B., Jiang, J. H., . . . Shi, Y. (2018). Incidence and risk factors for retrograde type A dissection and stent graft-induced new entry after thoracic endovascular aortic repair. *Journal of Vascular Surgery, 67*(4), 1026-1033. e1022. doi: 10.1016/j.jvs.2017.08.070

Ma, T., Dong, Z. H., Wang, S., Meng, Z. Y., Chen, Y. Y., & Fu, W. G. (2018). Computational investigation of interaction between stent graft and aorta in retrograde type A dissection after thoracic endovascular aortic repair for type B aortic dissection. *Journal of Vascular Surgery, 68*(6), 14S-21S. e12. doi: 10.1016/j.jvs.2018.06.008

Mao, S. S., Ahmadi, N., Shah, B., Beckmann, D., Chen, A., Ngo, L., . . . Budoff, M. J. (2008). Normal thoracic aorta diameter on cardiac computed tomography in healthy asymptomatic adults: impact of age and gender. *Academic Radiology, 15*(7), 827-834. doi:10.1016/j.acra.2008.02.001

Martufi, G., Di Martino, E. S., Amon, C. H., Muluk, S. C., & Finol, E. A. (2009). Three-Dimensional Geometrical Characterization of Abdominal Aortic Aneurysms:

Image-Based Wall Thickness Distribution. *Journal of Biomechanical Engineering, 131*(6). doi:10.1115/1.3127256

Menichini, C., Pirola, S., Guo, B., Fu, W., Dong, Z., & Xu, X. Y. (2018). High wall stress may predict the formation of stent-graft–induced new entries after thoracic endovascular aortic repair. *Journal of Endovascular Therapy, 25*(5), 571-577. doi: 10.1177/1526602818791827

Miller, K., Mufty, H., Catlin, A., Rogers, C., Saunders, B., Sciarrone, R., . . . Wittek, A. (2020). Is There a Relationship Between Stress in Walls of Abdominal Aortic Aneurysm and Symptoms? *Journal of Surgical Research, 252*, 37-46. doi:https://doi.org/10.1016/j.jss.2020.01.025

Nathan, D. P., Xu, C., Pouch, A. M., Chandran, K. B., Desjardins, B., Gorman, J. H., . . . Jackson, B. M. (2011). Increased wall stress of saccular versus fusiform aneurysms of the descending thoracic aorta. *Annals of Vascular Surgery, 25*(8), 1129-1137. doi: 10.1016/j.avsg.2011.07.008

Nienaber, C. A., & Powell, J. T. (2011). Management of acute aortic syndromes. *European Heart Journal, 33*(1), 26-35. doi: https://doi.org/10.1093/eurheartj/ehr186

Orabi, N. A., Quint, L. E., Watcharotone, K., Nan, B., Williams, D. M., & Kim, K. M. (2018). Distinguishing acute from chronic aortic dissections using CT imaging features. *The International Journal of Cardiovascular Imaging*, 1-10. 34(11):1831-1840. doi: 10.1007/s10554-018-1398-x

Pantaleo, A., Jafrancesco, G., Buia, F., Leone, A., Lovato, L., Russo, V., . . . Pacini, D. (2016). Distal stent graft-induced new entry: an emerging complication of endovascular treatment in aortic dissection. *The Annals of Thoracic Surgery, 102*(2), 527-532. doi: 10.1016/j.athoracsur.2016.02.001

Patterson, B. O., Cobb, R. J., Karthikesalingam, A., Holt, P. J., Hinchliffe, R. J., Loftus, I. M., & Thompson, M. M. (2014). A systematic review of aortic remodeling after endovascular repair of type B aortic dissection: methods and outcomes. *The Annals of Thoracic Surgery, 97*(2), 588-595. doi: 10.1016/j.athoracsur.2013.07.128

Peterss, S., Mansour, A. M., Ross, J. A., Vaitkeviciute, I., Charilaou, P., Dumfarth, J., . . . Elefteriades, J. A. (2016). Changing Pathology of the Thoracic Aorta From Acute to Chronic Dissection. *Literature Review and Insights, 68*(10), 1054-1065. doi:10.1016/j.jacc.2016.05.091

Raghavan, M. L., Webster, M. W., & Vorp, D. A. (1996). Ex vivo biomechanical behavior of abdominal aortic aneurysm: assessment using a new mathematical model. *Annals of Biomedical Engineering, 24*(5), 573-582. doi:10.1007/bf02684226

Ranga, A., Mongrain, R., Biadilah, Y., & Cartier, R. (2007). *A compliant dynamic FEA model of the aortic valve.* Paper presented at the 12th IFToMM World Congress, Besançon, France.

Roccabianca, S., Figueroa, C. A., Tellides, G., & Humphrey, J. D. (2014). Quantification of regional differences in aortic stiffness in the aging human. *Journal of the Mechanical Behavior of Biomedical Materials, 29*, 618-634. doi:https://doi.org/10.1016/j.jmbbm.2013.01.026

Shang, E. K., Nathan, D. P., Sprinkle, S. R., Fairman, R. M., Bavaria, J. E., Gorman, R. C., . . . Jackson, B. M. (2013). Impact of wall thickness and saccular geometry on the computational wall stress of descending thoracic aortic aneurysms. *Circulation, 128*(11 suppl 1), S157-S162. doi: 10.1161/circulationaha.112.000200

Shang, E. K., Nathan, D. P., Sprinkle, S. R., Vigmostad, S. C., Fairman, R. M., Bavaria, J. E., . . . Jackson, B. M. (2013). Peak wall stress predicts expansion rate in descending thoracic aortic aneurysms. *The Annals of Thoracic Surgery, 95*(2), 593-598. doi: 10.1016/j.athoracsur.2012.10.025

Simsek, F., & Kwon, Y. (2015). Investigation of material modeling in fluid-structure interaction analysis of an idealized three-layered abdominal aorta: aneurysm initiation and fully developed aneurysms. *Journal of Biological Physics, 41*(2), 173-201. doi:10.1007/s10867-014-9372-x

Singh, S. D., Xu, X. Y., Pepper, J. R., Treasure, T., & Mohiaddin, R. H. (2015). Biomechanical properties of the Marfan's aortic root and ascending aorta before and after personalised external aortic root support surgery. *Medical Engineering & Physics, 37*(8), 759-766. doi:https://doi.org/10.1016/j.medengphy.2015.05.010

Spinella, G., Finotello, A., Conti, M., Faggiano, E., Gazzola, V., Auricchio, F., . . . Pane, B. (2018). Assessment of geometrical remodelling of the aortic arch after hybrid treatment. *European Journal of Cardio-Thoracic Surgery, 55*(6), 1045-1053. doi: 10.1093/ejcts/ezy397

Sze, D. Y., Van Den Bosch, M. A., Dake, M. D., Miller, D. C., Hofmann, L. V., Varghese, R., . . . Mitchell, R. S. (2009). Factors portending endoleak formation after thoracic aortic stent-graft repair of complicated aortic dissection. *Circulation: Cardiovascular Interventions, 2*(2), 105-112. doi: https://doi.org/10.1161/CIRCINTERVENTIONS.108.819722

Tan, W. T., Mokhtraudin, M. J. M., Liew, Y. M., Johari, N. H., & Lim, E. (2019). *Biomechanical analysis of distal stent graft induced new entry (SINE) formation in aortic dissection patient.* Paper presented at the 6th International Conference on Computational and Mathematical Biomedical Engineering, Sendai city, Japan: Tohoku University. http://www.compbiomed.net/2019/cmbe-proceedings.htm

Thubrikar, M. J., Al-Soudi, J., & Robicsek, F. (2001). Wall stress studies of abdominal aortic aneurysm in a clinical model. *Annals of Vascular Surgery, 15*(3), 355-366. doi: https://doi.org/10.1007/s100160010080

Trimarchi, S., & Eagle, K. A. (2016). Thoracic endovascular aortic repair in acute and chronic type B aortic dissection. In: JACC: Cardiovascular Interventions. doi: 10.1016/j.jcin.2015.11.033

van Bakel, T., Nauta, F., Conti, M., Romarowski, R., Morganti, S., van Herwaarden, J., . . . Trimarchi, S. (2019). Novel Understanding on Thoracic Aortic Diseases from Bioengineering Concepts. In *Surgical Management of Aortic Pathology* (pp. 141-148): Springer.doi: 10.1007/978-3-7091-4874-7_9

van Bakel, T. M., Figueroa, C. A., van Herwaarden, J. A., & Trimarchi, S. (2018). Commentary: Challenges of Thoracic Endovascular Aortic Repair for Type B Aortic Dissection. *Journal of Endovascular Therapy, 25*(5), 578-580. doi: https://doi.org/10.1177/1526602818795153

van Bakel, T. M., Romarowski, R. M., Morganti, S., van Herwaarden, J. A., Moll, F. L., de Beaufort, H. W., . . . Trimarchi, S. (2018). Blood Flow after Endovascular Repair in the Aortic Arch: A Computational Analysis. *Aorta (Stamford), 6*(3), 81-87. doi:10.1055/s-0039-1683771

van Bakel, T. M. J., Arthurs, C. J., Nauta, F. J. H., Eagle, K. A., van Herwaarden, J. A., Moll, F. L., . . . Figueroa, C. A. (2018). Cardiac remodelling following thoracic endovascular aortic repair for descending aortic aneurysms†. *European Journal of Cardio-Thoracic Surgery*, ezy399-ezy399. doi:10.1093/ejcts/ezy399

Venkatasubramaniam, A. K., Fagan, M. J., Mehta, T., Mylankal, K. J., Ray, B., Kuhan, G., . . . McCollum, P. T. (2004). A Comparative Study of Aortic Wall Stress Using Finite Element Analysis for Ruptured and Non-ruptured Abdominal Aortic Aneurysms. *European Journal of Vascular and Endovascular Surgery, 28*(2), 168-176. doi:https://doi.org/10.1016/j.ejvs.2004.03.029

Weng, S.-H., Weng, C.-F., Chen, W.-Y., Huang, C.-Y., Chen, I. M., Chen, C.-K., . . . Shih, C.-C. (2013). Reintervention for distal stent graft-induced new entry after endovascular repair with a stainless steel-based device in aortic dissection. *Journal of Vascular Surgery, 57*(1), 64-71. doi:https://doi.org/10.1016/j.jvs.2012.07.006

Yeh, H. H., Rabkin, S. W., & Grecov, D. (2018). Hemodynamic assessments of the ascending thoracic aortic aneurysm using fluid-structure interaction approach. *Medical & Biological Engineering & Computing, 56*(3), 435-451. doi: 10.1007/s11517-017-1693-z

Yu, X., Wang, Y., & Zhang, Y. (2018). Transmural variation in elastin fiber orientation distribution in the arterial wall. *Journal of the Mechanical Behavior of Biomedical Materials, 77*, 745-753. doi: 10.1016/j.jmbbm.2017.08.002

Zhao, Y., Yin, H., Chen, Y., Wang, M., Zheng, L., Li, Z., & Chang, G. (2018). Restrictive bare stent prevents distal stent graft-induced new entry in endovascular repair of type B aortic dissection. *Journal of Vascular Surgery, 67*(1), 93-103. doi:https://doi.org/10.1016/j.jvs.2017.04.066

Zhou, Y., Wang, W. C., Zhang, X. M., Yang, C., Zheng, J., Yang, L., . . . Yang, Y. (2018). Aortic remodelling after thoracic endovascular aortic repair for acute and subacute type B aortic dissection. *Quant Imaging Med Surg, 8*(4), 391-398. doi:10.21037/qims.2018.05.03

Zhu, J., Zhao, L., Dai, X., Luo, Y., Fan, H., Feng, Z., . . . Hu, F. (2018). Fenestrated Thoracic Endovascular Aortic Repair Using Physician Modified Stent Grafts for Acute Type B Aortic Dissection with Unfavourable Landing Zone. *Eur J Vasc Endovasc Surg, 55*(2), 170-176. doi:10.1016/j.ejvs.2017.11.012

Ziganshin, B. A., & Elefteriades, J. A. (2019). Mechanics of the Thoracic Aortic Wall. In O. H. Stanger, J. R. Pepper, & L. G. Svensson (Eds.), *Surgical Management of Aortic Pathology: Current Fundamentals for the Clinical Management of Aortic Disease* (pp. 149-162). Vienna: Springer Vienna.

LIST OF PUBLICATIONS AND PAPERS PRESENTED

WT Tan, MJM Mokhtarudin, YM Liew, NH Johari, & E Lim (2019). Biomechanical analysis of distal stent graft induced new entry (SINE) formation in aortic dissection patient. In P. Nithiarasu, M. Ohta & M. Oshima (Eds.),*CMBE2019 Conference: 6th International Conference on Computational and Mathematical Biomedical Engineering: Computational study on stent: from material to application: (pp. 747-750).*Sendai city, Japan: Tohoku University.Retrieved from http://www.compbiomed.net/2019/cmbe-proceedings.htm

Tan, W. T., Liew, Y. M., Mohamed Mokhtarudin, M. J., Pirola, S., Wan Ab Naim, W. N., Amry Hashim, S., Xu, X. Y., & Lim, E. . Effect of vessel tortuosity on stress concentration at the distal stent vessel interface: possible link with new entry formation through biomechanical simulation. Journal of Biomechanical Engineering.